UNIVERSITY OF SOUTHAMPTON

FACULTY OF ENGINEERING, SCIENCE AND MATHEMATICS

SCHOOL OF CIVIL ENGINEERING AND THE ENVIRONMENT

WAVE DIFFRACTION IN MICRO MODELS

MARIA VRYONIDI

A dissertation submitted in partial fulfillment of the degree of MSc in Engineering in the Coastal Environment by instructional course

September 2011

Summary

Ports and coasts have been playing an important role in the world economy through the years. When planning a port, the study of the diffraction phenomenon is required, as the entrance of the harbour has to be properly designed to avoid any kind of problems. For that reason the wave height distribution has to be considered. Physical models are able to study the coastal processes, such as wave propagation and diffraction that affect the tranquility of the harbor, but require a lot of time and money.

Micro models (very small – table top physical models) can be the low cost alternative to the large scale physical models and although they were criticized a lot, their use for coastal studies seems to be a clever and quick option. Although micro models were criticized about their validity due to the scale effects, the literature concludes that the micro modeling of non-breaking waves is possible for water depths larger than 0.03m and wave periods longer than 0.35sec, when the scale effects can be negligible.

Stagonas (2010) was the first to explore the potential of small-scale physical models of waves (micro-models) as a modeling tool for coastal engineers and scientists. The current thesis focuses on the diffraction phenomenon, uses the data of Stagonas' experiments and will try to establish the validity of micro models by comparing their results to those exported by the theoretical and numerical solutions.

A novel mapping method called Particle Image Velocimetry (PIV), that allows the measurement of the whole wave field rather than using single point measurements (as it is usually applied in physical model tests) was used to map the wave field. The velocities of the floating particles were used to extract wave heights (incident and diffracted). The most important is that the calculations take into account the wave reflection occurring in front of the breakwater. This process makes the wave components in front of the breakwater proceeding in the opposite direction than the other components and increases the wave height in front of the breakwater.

The theoretical solution of Penny and Price 1944 &1952 was used along with the vastly used numerical model, Mike 21 (by DHI) to simulate the different experiments of a single breakwater, a breakwater gap and the Ostia port in Italy. The three methods (experimental-micro modeling, theoretical and numerical) are compared to conclude that they agree in most of the cases. The value of the diffraction coefficient is similar for the three different methods in most of the locations in the experimental basin. According to that, it can be concluded the micro modeling of the diffraction phenomenon is valid. The wave mapping method in combination with wave micro-models appears to be an attractive way of studying the wave propagation and the diffraction phenomenon.

Acknowledgement

This dissertation could not have been written without Dimitris Stagonas who not only served as my supervisor but also encouraged and challenged me throughout my academic program. He and the other faculty members guided me through the dissertation process, never accepting less than my best efforts.

I would also like to thank Mr. Karambas for the provision of the theoretical solutions.

I wish to thank all those who helped me, especially my parents for the funding and the huge support and the flat mates and friends for their help and company. Without them, I could not have completed this project.

Table of Contents

List of figures

List of tables

List of abbreviations

BEM:	Boundary Element Method
BW:	Boussinesq Waves
LSPIV:	Large Scale Particle Image Velocimetry
LSW:	Liquid Surface Wave
MBM:	Movable Bed Model
PIV:	Particle Image Velocimetry
USACE:	U.S Army Corps of Engineers

List of symbols

Symbol	Unit	Description
a	m or cm	Wave amplitude
b	m or cm	Width of the tank
B	m or cm	Breakwater gap
c	m/sec	Wave celerity
d	m or cm or m	Water depth
f	1/sec	Wave frequency
$F(r, \vartheta)$	-	Modulus
Fr	-	Froude number
g	m/sec^2	Acceleration due to gravity
h	m or cm	Water depth
h_A	m or cm	Layer thickness
H_i	m or cm	Incident Wave height
H_d	m or cm	Diffracted Wave height
i	-	Bed Slope
k	-	Wave number
K’	-	Diffraction coefficient
L	m or cm	Wave length
n_s	m or cm	Surface elevation
r	m or cm	Distance
R	m	Hydraulic radius
R_e	-	Reynolds number
R_x, R_y	m	Radii of curvature
t	sec	Time
T	sec	Wave period
u	m/sec	Particle velocity
v_A	m/sec	Wave run up velocity
V	m/sec	Wave velocity
W_e	-	Weber number
x	m or cm	Vertical distance
x_p	m or cm	Horizontal distance in flume
z	m or cm	Horizontal distance
α	-	Damping constant
β	Degrees	Angle between r and the breakwater
ϑ	Degrees	Incident wave propagation angle
μ	$N*s/m^2$	Dynamic viscosity
ν	m^2/sec	Kinematic viscosity
ρ	Kg/m^3	Fluid density
σ	N/m	Surface tension
ω	rad/sec	Angular frequency

Introduction

Since the ancient years, most of the earth's popularity lives near the coasts. The big ports that were built, had converted the small towns into large commercial cities. Due to the rapid and huge development, the climate changed and continues to do so. Nowadays, the natural phenomena occur more frequently than in the past. As the sea level rises, threatens the ports and cities that need to be protected against wave action and other disastrous events.

For those reasons, the Coastal engineers have an important role to play. The design of coastal structures and proposing measures suitable for each situation, are today more than important. To meet these challenges, the engineers have to investigate, compare and finally use all the tools developed in the past, such as numerical, theoretical and physical models. Those tools are able to predict the reaction of their proposed structures with the natural environment in order to achieve the 'best' solution!

The disturbance inside harbor basins is one of the most important factors when engineers are to select construction sites and determine the optimum harbor layout in relation to predefined criteria for acceptable wave disturbance, ship movements, mooring arrangements and handling downtime. In this project the wave propagation and diffraction will be investigated using micro models (very small-scaled, Tabletop, physical models (1:20,000)) as first introduced by Davinroy in 1994 (U.S Army Corps of Engineers (USACE)). Micro-models, due to their small size can be the cheap and flexible attractive to the expensive large-scale physical models. On the other hand the use of micro models was criticized (Maynord 2006), as many variables (especially the sediment movement) are impossible to be reproduced in such small scales.

Wave micro-models were seldom used for coastal research; from Beckett and Marshall (1983). Rankine (1991) used very small scale (1:2000) hydraulic models to model the tidal flow effects in harbors. Stagonas in 2010 used micro models to study the diffraction phenomenon along with other coastal processes.

The current thesis is studying the water wave diffraction phenomenon (taking into account the reflection caused by the presence of the breakwater) using micro models and will compare the results to those extracted by the theoretical and numerical (Mike 21) solutions in order to test the validity of micro models. If the results (diffraction coefficient) of the three methods 'agree', the micro models can describe the diffraction phenomenon, and so the small-scaled models can be used for the engineering studies of diffraction and why not in any other coastal study.

The first chapter is a review of any past work that has been carried out covering the subject. Chapter two outlines the work that was done to export the results that are

presented in chapter three. The Ostia port in Rome has been modeled in order to add to the research and it is discussed individually in chapter four. The conclusion at the end puts together he findings.

Aim

When planning a port, the disturbance inside the harbor basins is important in order to determine the 'best' layout. For that reason the study of the diffraction phenomenon is both useful and important. The project investigates the wave propagation and the diffraction phenomenon when using micro models. It is true that small-scale models violate most of the conditions that need to be met for the model, to accurately present the prototype. However, in this case (the water wave diffraction phenomenon) when sediment transport is not considered, only the effects of small scale on the fundamental wave processes are investigated.

The current project compares the results given by the micro model solution (experimental) to the existing literature (Penny & Price 1944) and numerical solution given by a vastly used software like Mike 21 Boussinesq model (by DHI), to test the validity of micro models. If micro models are able to describe the wave diffraction around a single breakwater and through a breakwater gap, then they can be used to suggest new ideas, test design options and finally solve engineering problems.

1. Literature review

1.1 Physical models

A physical model is a smaller or larger physical copy of an object. According to Hughes (1993) physical models are reproducing a physical system in the laboratory so that the major forces acting in nature are represented in the model in the correct proportion. They can give a good simulation of the reality as they include all the processes that take place in the reality. They also allow visualization of the inner parts of the process that normally is invisible. The purpose of a physical model on a smaller scale is to have a better overview of the real situation and on a larger scale is to see the structure of things that are normally too small to see properly or to see at all.

Prototype is called the situation that is modeled. Scale is the constant proportion of measurable characteristics between the model and the prototype (Yalin 1971). In many cases the similarity is only approximate or even intentionally distorted. Sometimes the distortion is systematic with e.g. a fixed scale horizontally and a larger fixed scale vertically. Distorted models are those whose horizontal length scale is different from the vertical, and so the model is not geometrically similar to the prototype.

Instrumented physical models are the most effective way of investigating fluid flows such as around hydraulic structures. These models are scaled in terms of both geometry and important forces, for example using Froude number or Reynolds number scaling.

According to Dalrymple (1985) the advantages of physical models are:

1. They integrate the equations governing the processes without making simplified assumptions as in the analytical or numerical models. As mathematical modeling is limited by the accuracy of the mathematical relationships, physical models give the chance to monitor and measure the physics in a controlled environment (Le Mehaute 1990).
2. Due to the small size of the model, the data collection is easier and cost effective comparing to the field data collection.
3. Visual feedback can be collected.
4. They allow simulating rare environmental conditions.

Le Mehaute (1990) adds to the previous:

1. Physical models add reliability and credibility to the decision making process.
2. Nowadays, using new techniques allow discovering the physical relationships of fluid flow, treating large quantity of data and establishing more complex equations.
3. They allow reproduction of complex boundary conditions.
4. The nonlinear effects are almost the same in model and prototype.

The main disadvantages of physical modeling are:

1. Scale effects occur in those models that are smaller than the prototype. For example viscous forces in the models are larger than in nature (prototype)! The ability to simulate the relevant forces in the model at a proper scale is dictated by the scaling (similitude) criteria.
2. Laboratory effects cause the differences between the prototype and the model, due to inability to create realistic forcing conditions because of the limitations of the laboratory facilities (solid boundaries and wave generators).
3. Physical models sometimes miss the forcing functions and boundary conditions that are present in nature and have to be assessed, for example the wind shear stress in the free surface.
4. They are sometimes more expensive than numerical models. The high maintenance and operation costs make the use of physical models difficult.
5. Creating the physical model is time demanding, as much time is spent for its preparation and operation.

According to Yalin (1989), 'Physical model is a precision device used to predict the behavior of physical phenomenon. It can be reliable only if is designed correctly, but if not, then it is wrong in principle and the most sophisticated instrumentation and measurement methods can only increase the accuracy of wrong predictions'.

Due to the previous (large cost, time required and similitude problems), it can be concluded that the physical modeling can "only" be used for large projects when only the final decision can be tested.

1.2 Micro models

Considering all those reasons that were stated earlier, the use of physical models could be replaced with micro models, physical models that have scale smaller than 1:50 and can be put in a desk. According to Maynord (2006) the micro-model of a river is an extremely small physical model, having a movable bed, varying discharge, and numerous innovations in order to answer the river engineering questions. Micro modeling can be a cheap, qualitative and flexible alternative to the large scale models due to the small experiment costs, simulation time and space requirement. Furthermore, there is no need of trained people (scientists) to use those small models.

The development of river micro model (scale of 1/20000) took place in St. Luis district in October 1994 from the new facility called the Applied River Engineering Centre (US Army Corps of Engineers (USACE)), by Rob Davinroy to study the Mississippi River side channel restoration. The simulated hydrographic/ sediment response of the alluvial system took place in the tabletop flume. 'The micro model can qualitatively predict the average expected sediment response of a real waterway' (Claude Strauser 1998). Davinroy's report investigates the sedimentation, using a physical hydraulic micro model, to evaluate existing conditions and various design measures to improve the environment in the Mississippi River. A variety of environmental design alternatives were submitted having the goal to evaluate the positive impacts of them. The challenge was to create desirable biological diversity and ensure a reliable navigation channel. How effective was each plan, was evaluated by comparing the plan results to the base test condition.

Micro models were mostly used for river navigation design such as dikes, revetments, dredging studies, dredge disposal impacts, small river design, bridge scour studies and educational applications. They have been also used in geomorphic studies, such as meandering, aggradation and degradation. As they allow visualizing and explaining complex phenomena (such as sediment transport), clearly demonstrate what a river structure will do in any reach of the river, micro modeling can be a useful educational tool. The usual goal of micro model studies was to provide solutions for the reduction of maintenance and dredging and improve navigability.

Claude Strauser (Chief of Potamology Section (1998)) supports the use o micro models; 'the technology of micro modeling is continuing to evolve. Laser technology and electronic automation are making it more and more efficient. There's little doubt that micro modeling is an important innovation. This tool will enhance the science of river engineering well into the 21st century'.

Micro models had a small use in coastal research; as they were only used for tidal flow effects on ports (Beckett and Marshall 1983 and Nece 1985).

Beckett and Marshall (1983) used a very small-scale hydraulic model, for the investigation of tidal flow effects on the Muara deep-water port at Brunei. The physical model that was constructed inside a rocking tray had a Plasticine movable bed and simulated tidal flows to check whether the harbour could be economically maintained and compares the effect of different training works. The model tests were successful in identifying the best harbour configurations and the recommended scheme was then studied in a large scale Movable Bed Model (MBM).

Nece (1985) similarly developed a small-scale boat harbor to provide answers on tidal flushing problems, as the numerical models couldn't describe the complex flow field. The author attributed the failure of the model to predict the prototype to the stratification and wind effects that were not taken into account. He concluded that such small-scale model cannot give accurate quantitative answers but they can be used to compare various design options and their effect on internal circulation patterns.

1.3 Diffraction

As micro models were seldom used for coastal studies, Stagonas (2010) in his thesis used those small hydraulic models to study the coastal processes, such as wave propagation and diffraction around a single breakwater and a breakwater gap.

When the water waves are propagated into the sheltered region created by a breakwater, a portion of those regular waves are interrupted by the breakwater. When a structure (breakwater) is present, a part of the wave will move past the tip and be a source of flow energy in the defended area (diffraction by Wiegel 1976) and a part of it will be reflected. Wave Diffraction is the phenomenon where energy is transferred along the wave crests (from Region II into Region I) (figure 1.1). Wave energy transfer cannot occur and so the region in the lee of the breakwater is calm and the waves would pass unchanged in form and height. In front of the barrier apart from the incident waves, reflected waves exist due to the reflection of the incident waves by the barrier (region III). The superposition of incident and reflected waves, when the incident waves approach the breakwater obliquely, results in the appearance of short-crested waves. If the waves approach perpendicular to the breakwater, a standing wave will occur.

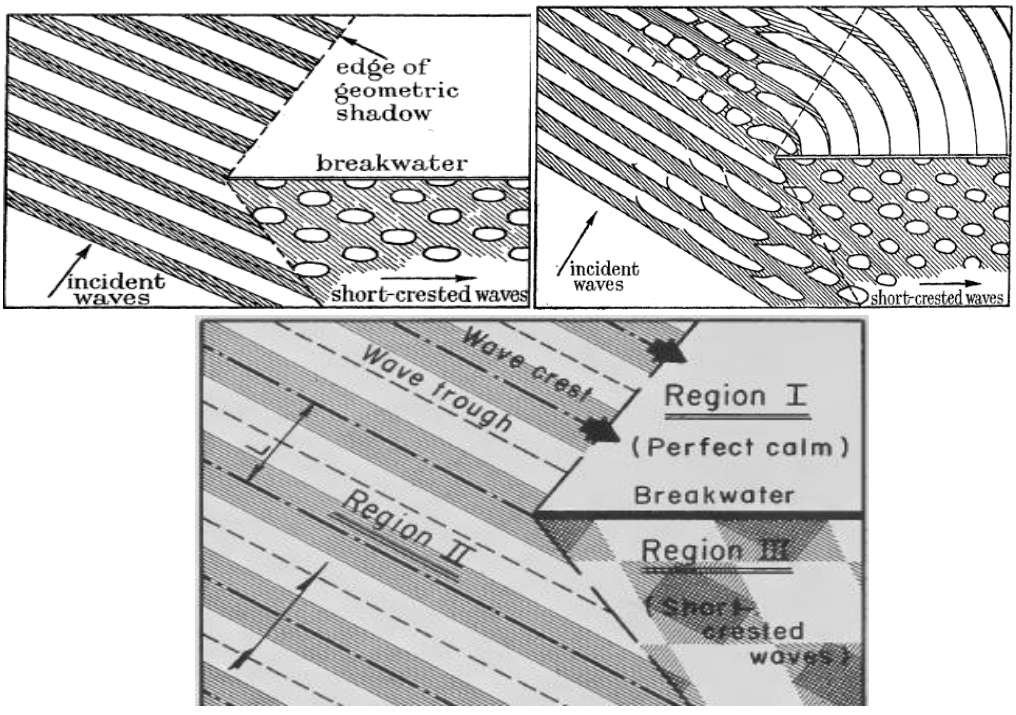

Figure 1.1: Top: Wave propagation and energy transfer through the regions when an obstacle (breakwater) is present- the diffraction effects; Below: No diffraction.
Source: Shore Protection Manual 1984 (2-76).

The diffraction phenomenon has to be taken into account, as its effects are important for many reasons. For example, when planning a port or a sheltered bay, the entrance of the

harbour has to be properly designed to avoid problems as silting and harbour resonance. For that reason, the wave height distribution has to be considered in the areas affected by the diffraction of natural or man-made structures that protect the area from the incident waves. Scientists developed diffraction theories that follow assumptions below to investigate the principles of diffraction:

1. Water is an ideal fluid (Inviscid and incompressible).
2. The small amplitude waves can be calculated by the linear wave theory.
3. The flow is irrotational and follows a potential function, which satisfies the Laplace equation.
4. The water depth shoreward of the breakwater is constant.

Penny and Price (1944) showed that Somerfield's solution of the optical diffraction could also be the solution for water wave diffraction problem.

There are two types of the wave diffraction problem:

1. The passage of waves around the end of a semi-infinite impermeable breakwater. The experiments of Putnam and Arthur (1948) concluded that the experimental and theoretical value of Penny and Price for the diffraction coefficient (K') around a single breakwater, agree. Outside the geometric shadow the experimental wave heights were smaller than the theoretical. Wiegel (1962) also used a theoretical approach to study wave diffraction around a single breakwater.
2. The passage of waves through a breakwater gap (Blue and Johnson (1949), Carr and Stelzriede (1951), Johnson (1952)). Blue and Johnson (1949) reported on experiments with diffraction at a breakwater gap for deep and shallow water waves. The results of experiments by Blue and Johnson (1949) agree to those by Putnam and Arthur (1948) regarding the values of K'. The experimental and theoretical wave patterns for deep and shallow-water waves were close. The experimental wave patterns showed a more sharply convex crest shape than the theoretical ones. Irregularities in the experimental wave patterns occurred due to the wave steepness. It was observed that the steeper the incident wave, the greater was the velocity increase along the diffraction axis and outside the geometric shadow and the more irregular being the diffraction pattern. Within the geometric shadow the theoretical values of wave height are within about 10% of the actual value. The theoretical wave heights exceed the actual heights.

In general, the theoretical solutions are conservative; the predicted wave heights in the lee of the breakwater are slightly larger than in reality (Johnson 1952). Far from the breakwater probably the refraction effects are dominant over the diffraction.

Recently, Pos and Kilner (1987) compared the experimental results to the finite and infinite element (program WAVE) and analytical results. They concluded that the measured wave height in the shadow zones (sheltered by the breakwater) is larger than the theoretical, while outside that zone is smaller than the theoretical. This is due to secondary waves generated at the breakwater and wave orthogonal spreading at the centerline respectively.

Dalrymple and Martin (1990) used the eigenvalue - expansion approach and two variational methods to study the diffraction and refraction problem due to inline segments of offshore breakwaters. The approximate method of Lamb (1932) allowed calculating the diffraction coefficient only for short waves. Dalrymple and Martin used the variational methods (following Schiwnger and Saxon 1968) that provided valid estimations for all the wavelengths (smaller or bigger than the breakwater gap). These methods were then compared to the eigenfunction expansion method (when $0<k_b<p$, where kb is the dimensionless channel width) to conclude that for the smallest values of the dimensionless gap widths (l/b) the variational approaches bracket the eigenfunction method. But as the gap increases the variational method becomes better. Specifically, Lamb's method compares well with the eigenfunction solution (can calculate accurately the refraction coefficient) when l/b and k_b are small (when the wavelength is bigger than the gap), but for smaller wavelengths only the eigenfunction can be used to calculate the refraction coefficient, as the variational method is not valid.

Abul-Azm and Williams (1997) used the eigenfunction expansion solution of Dalrymple and Martin to study the oblique wave diffraction by a detached offshore breakwater system. Numerical results in the form of contour maps of the wave height are exported for different wave and breakwater parameters. Their results in all cases showed a good agreement with other solutions in the literature (single breakwater (Johnson 1952), isolated, finite breakwater segment (Goda et al. 1971), segment breakwater (Huygens and Verhoeven 1992)).

Briggs et al. (1995) used a physical model in the wave basin to experiment the diffraction caused by semi-infinite breakwaters. That paper contains a complete set of experimental data on the refraction and diffraction of multidirectional random waves through a breakwater gap. They have also studied the effects of the size of the gap and the wave direction on the diffraction coefficient.

Kim and Lee (2009) implemented numerical simulations based on the Polynomial approximation solution to obtain the results in the water wave diffraction problem by breakwater gap for various wave incidences. They resulted that the Polynomial approximation solution has excellent accuracy and agreements with the results obtained by the Fresnel integral, and reduces computational time by 73.6%. They finally suggested that the Polynomial approximation approach might be efficiently used in many practical situations to predict wave fields in the shadow region of a breakwater.

Kim and Lee (2010) reviewed the polynomial approximations and studied the diffraction problems of insular breakwaters, to overcome the long calculation time through the Fourier series and the eigenvalue expansion approach and the difficulty to set boundary conditions in complex harbors. They compared the analytical solutions based on Fresnel integral and Polynomial approximation solution of Fresnel integral, to the numerical solutions of Boundary element method (BEM) based on boundary integral equation. They concluded that in all cases excellent agreement was made between polynomial equations and the Fresnel integrals. The numerical solution also agrees with the analytical, apart of the area behind the breakwater, where the numerical solution gives a slightly smaller diffraction coefficient than the analytical.

Y. - X. Yu et al (1998) created a physical model to study the combined refraction and diffraction effects of waves through a breakwater gap for different incident angles, regular and random waves with narrow and broad frequency and direction spreading.

In order to take into account the reflection of waves when reaching a structure, Kim and Suh (2008) had derived analytic solutions for water wave scattering by a semi-infinite breakwater or a breakwater gap of partial reflection. They examined the effect of the reflection coefficient at the front face of the breakwater to conclude that when the reflection coefficient is reduced, the standing wave height in front of the breakwater is also reduced along with the wave agitation at the port entrance. The assumption made, was that the front face of the breakwater is of partial reflection while the back face is of perfect reflection. The solution can be used for a breakwater of arbitrary reflection coefficients at both front and back faces, for normally incident waves.

Kim et al (2010) extended the previous solution to obliquely incident waves. Their solutions were used to investigate how the reflection coefficient of the breakwater and the wave incident angle affect the tranquility of harbor entrance. The results were similar to their previous study.

1.3.1 Diffraction calculations

a. **Waves Passing around a Single Breakwater.** Wiegel (1962) and Johnson (1950) introduced the diffraction diagrams (figure 1.2) for a uniform depth adjacent to an impervious structure that show lines of equal wave height reduction. Wave height reduction is given in terms of a diffraction coefficient K' which is the ratio of the diffracted wave height at a point (x, y) to the incident wave height at the breakwater: $K'=H_d/H_i$. The diagrams illustrate the wave fronts and contours of equal diffraction coefficient for a semi-infinite, rigid breakwater for dimensionless wavelength. In order to use the diagrams it is needed to provide the characteristics of the wave (H, T, direction). Silvester and Lim (1968) and Larras (1966) suggested that each diffraction coefficient in the lee of the breakwater can be the sum of an incident and reflected term. The incident term represents the diffraction of the incident waves into the shadow zone and the second term represents the diffraction of the reflected waves from the seaward side of the breakwater into the shadow zone.

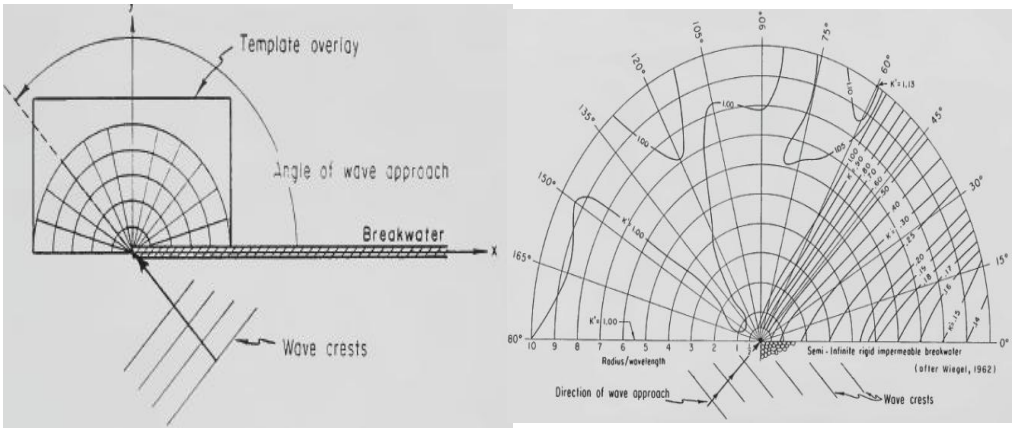

Figure 1.2: Left: Diffraction for a single breakwater normal incidence. Source: Shore Protection Manual (SPM) 1984, page 2-91.Right: Wave diffraction diagram for 45° wave angle. Source**:** Shore Protection Manual 1984, page 2-80.

b. **Waves Passing a Gap of Width Less Than Five Wavelengths at Normal Incidence.**

The diagrams (figure 1.3, by Johnson 1952) show lines of equal diffraction coefficient for gap/wavelength (B/L) ratios of 0.50, 1.00, 1.41 1.64, 1.78, 2.00, 2.50, 2.95, 3.82, and 5.00. Diffraction occurs at the two sides of the gap and the wave height changes are different from the single breakwater's situation.

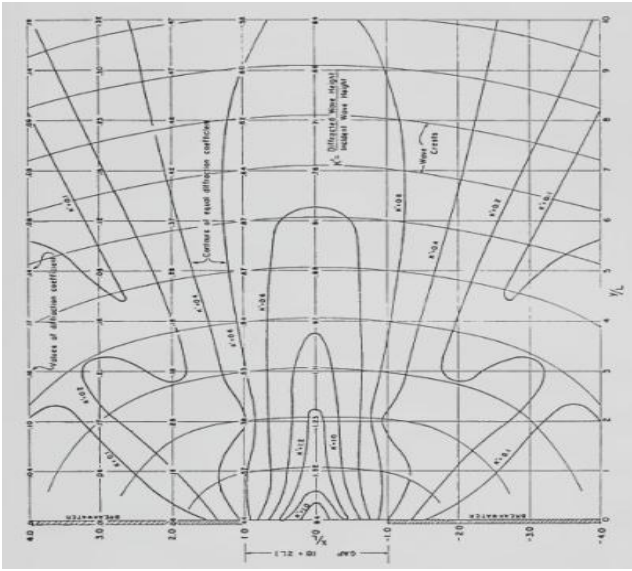

Figure 1.3: The Generalized diffraction diagram for a breakwater gap width of two wavelengths (B/L=2). Source**:** Shore Protection Manual 1984, page 2-93.

c. Waves Passing a Gap of Width Greater Than Five Wavelengths at Normal Incident.

For the situation where the gap is larger than five wavelengths, the diagram (figure 1.4) for a single breakwater with a 90° wave approach angle can be used to define the diffraction characteristics, as the diffraction effects in each breakwater are independent.

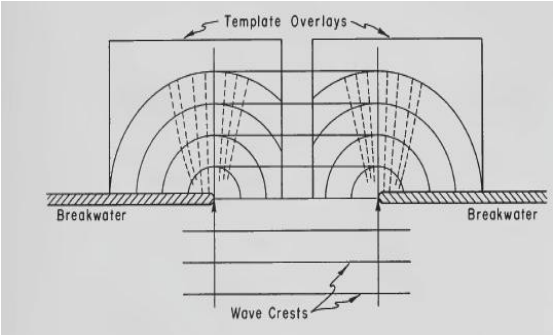

Figure 1.4: The Diffraction diagram for breakwater gap width > B/L=5.
Source**:** Shore Protection Manual (SPM) 1984, page 2-99.

d. Diffraction at a Gap-Oblique Incidence.

When waves approach at an angle, the diffracted wave characteristics differ from those resulting when waves approach normal to the axis. It can be considered that the gap's width is as its projection in the direction of incident wave travel, shown in figure 1.5.

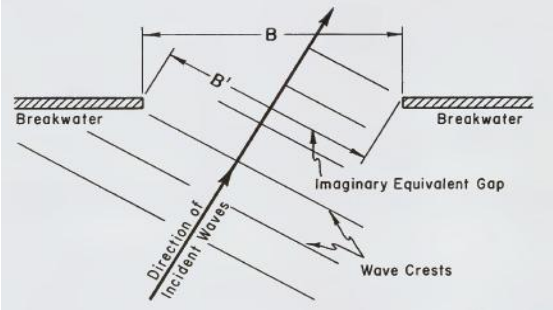

Figure 1.5: Wave incidence oblique to breakwater gap. Source**:** SPM 1984, page 2-99.

e. Other Gap Geometries.

Memos in 1976, 1980a, 1980b and 1980c developed an analytical solution for a diffraction of a breakwater gap, when the two breakwater legs have axes that intersect at an angle, for various angles of wave approach. In 1976 he presented the diffraction patterns for selected angles of approach.

f. Diffraction Around an Offshore Breakwater.

The diffraction pattern in the lee of a single breakwater is the result of superimposing two semi-infinite breakwater diffraction patterns. The combined diffraction coefficient is determined by putting together the two diffraction diagrams (figure 1.6). The solution is valid about two wavelengths behind and beyond the breakwater, while close to and in front of it, the solution is not valid.

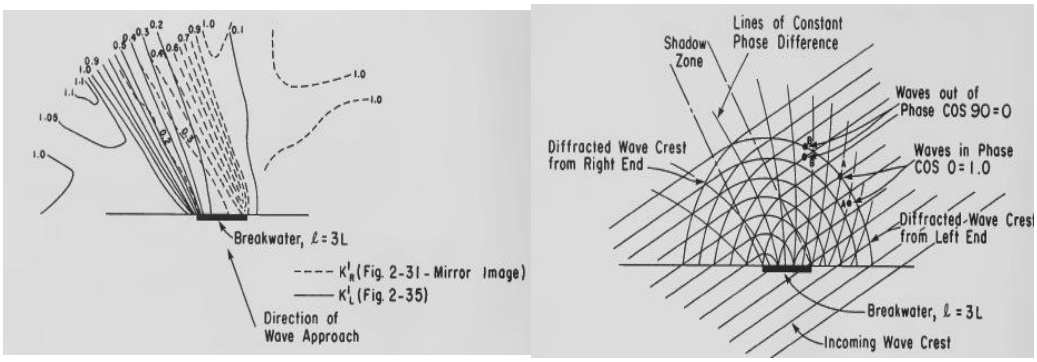

Figure 1.6: Approximate method for computing wave diffraction around an offshore breakwater. Source: SPM 1984, page 2-106.

Using the previous diagrams along with some tables, the calculation of the diffraction coefficient becomes much more easier. In this project, diagrams like the previous will be exported using micro models and numerical models, to investigate the diffraction in the area just behind the breakwater.

1.4 Laboratory and Scale effects

When using a physical - scaled model, the laboratory and scale effects have to be taken into account, so that the model can accurately reproduce the prototype. According to Le Mehaute (1990), a scale model has to:

1. Reproduce exactly the natural phenomenon under study.
2. Be consistent; give the same results under same conditions precisely.
3. Be sensitive, economical, have the ideal size and be completed in time.

As it has been already said, some of the advantages of scale models comparing to theory is that they are able to analyse complex boundary conditions and can reproduce the linear and non-linear forces, representing more accurately the reality.

Laboratory effects arise from the presence of solid boundaries (side walls) that do not exist in prototype and the inability to reproduce natural hydrodynamic forcing factors (waves & currents) (Svendsen & Haas 1999 & 2002). Those effects are minimized when using wave absorbers (Le Mehaute 1965).

As the physical model becomes smaller, its accuracy is also decreasing. A model is distorted when one of its scales is different from the other. In order for the physical model to accurately reproduce the prototype, similarity (kinematic, geometric and dynamic) has to be maintained (fulfilled). Similitude is achieved when all the factors that influence the reactions are in proportion between the prototype and the model, and those that are not, must be small or insignificant to the prototype (Hughes 1993). Requirements of similarity are the similitude criteria and the conditions of similarity. Similitude or scale criteria or scale laws are the mathematical conditions that must be met by the scale ratios between the prototype and the model (Hughes 1993). Scale ratio is the ratio of a parameter in prototype to its value in the model. Scale effects are the result of unsatisfactory reproduction of the phenomenon because of the too small scale. The geometrical similarity is fulfilled by the ratio ($1/N_L$) between all lengths in prototype and model. The fulfillment of the kinematical similarity requires identical time intervals for geometrical similar distances in prototype and model scale. This similarity can be fulfilled easily in a Froude model by reducing all time intervals by $1/ (L_N)^{0.5}$. The fulfillment of the dynamical similarity requires a constant ratio between all forces in model and prototype. Therefore, dynamical similarity is practically impossible in a scale model since all fluid properties (viscosity and surface tension) must be scaled simultaneously. This is

impossible since a geometrical scaled model requires different scales for friction forces and surface tension. The errors, which result from the inability to scale all fluid properties to model scale, are called scale effects (Hughes 1993).

The forces that need to be in similitude are the following and shown in figure 1.7 below:

I+G+P+F+E+C= 0; Inertia, Gravity, Pressure, Friction, Elastic and Capillary.

According to similitude, the following has to be maintained:

I/I' = G/G' = P/P' = F/F' = E/E' = C/C'

Complete similitude is impossible, as the previous condition cannot be obtained. So it is important to see which of these forces can be neglected and what are the scale effects.

Non- dissipative free surface flow short models are governed by inertia and gravity force. The ratio of Froude number has to be the same in prototype and scale model (Froude similitude):

$$\frac{V^2}{gL}(p) = \frac{V^2}{gL}(m)\left(\frac{V_m}{V_p}\right)^2 = \frac{L_m}{L_p} = \lambda$$

Where: λ is the geometric scale, m for model and p for prototype.

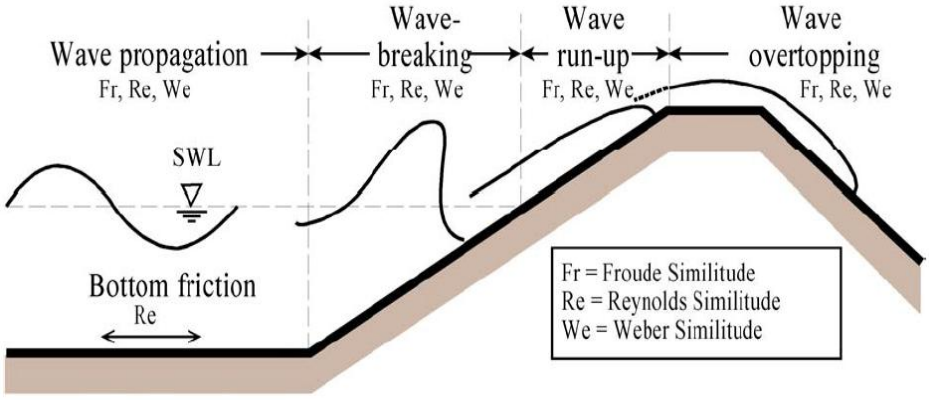

Figure 1.7: Processes and relevant similitude laws (Schuttrumpf 2001).

Wave propagation:

1. Froude number: expresses the influence of inertial and gravity forces.

$$Fr = \frac{V}{\sqrt{gL}} \qquad \text{(Equation 1)}$$

Where: V=velocity (for deep water $C = \frac{L}{T}$ and for shallow water V= c =$\sqrt{gd}$)

T = wave period, d = water depth.

Viscosity:

The fluid viscosity is accounted for the Reynolds number.

2. Reynolds number: is the ratio of the inertial to viscous forces.

$$Re = \frac{\rho LV}{\mu} \qquad \text{(Equation 2)}$$

Where: ρ = fluid density (Kg/m^3)

μ = dynamic viscosity ($N*s/m^2$, Pa*s or kg/m*s)

Surface tension:

3. Weber (We): expresses the influence of surface tension as follows:

$$We = \frac{\rho V^2 L}{\sigma} \qquad \text{(Equation 3)}$$

Where:

$\sigma =$ Surface tension; force acting in a direction tangent to the surface (force along a line of unit length, parallel to the surface but perpendicular to the line) so as to minimize the area and restore the surface to its original state. Surface tension is a property of the surface of a liquid that allows it to resist an external force. It has the dimension of force per unit length, or of energy per unit area (SI unit is joules per square meter).

The interfacial energy between a liquid and the substance that is in contact has to do with the difference between the interior attraction of the molecules of each phase and those at the surface of contact. This differs from the principle of conservation of energy: 'energy cannot be stored at the boundary'. The pressure difference between the two sides of the surface, times surface area results in a normal force. In order for the surface tension forces to cancel the force due to pressure, the surface must be curved. When all the forces are balanced, the resulting equation is known as the Young-Laplace equation:

$$\Delta p = \sigma \left(\frac{1}{Rx} + \frac{1}{Ry}\right) \quad \text{(Equation 4)}$$

Where:

Δp= pressure difference.

$\sigma =$ Surface tension.

R_x & R_y = radii of curvature in each of the axes that are parallel to the surface.

As the length of scale in the model decreases, the deviation increases, so wave damping occurs, which does not occur in the prototype. This has to be fixed, in order to have reliable measurements and results.

In short wave hydraulic models that are scaled according to Froude criterion, the non-similitude of viscous forces and surface tension forces can lead to scale effects such as reflection, transmission and energy dissipation. Wave reflection in the models tends to be smaller than in the prototype (Le Mehaute 1976) as in the model the friction is increased (the surface is rougher in the model). According to this, the losses due to friction are more in the model than in prototype.

In coastal engineering models, scale effects occur after assuming that gravity is the dominant force balancing the inertial forces. For that reason, the scaling is according to Froude and incorrectly scales the other forces (viscosity, surface tension and elasticity) that are believed to contribute little to the physical processes (Hughes 1993) although their values can be bigger in the model than in reality. Costa (1981,1984,1990) tested the 'secondary' forces (viscous, elastic, surface tension) influence and resulted that they are greater represented in the model than in the prototype.

The wave amplitude in physical modeling has to be maintained; not being reduced more than in the prototype. Wave attenuation occurs due to viscosity and surface tension while their influence in the field and laboratory will not be the same. As gravity is the largest and the most important force, the Froude criterion has to be fulfilled. Equality between the model and the prototype in terms of Froude criterion means that Weber and Reynolds criteria will be distorted and so the physical models do not accurately simulate the friction and surface tension effect. The simultaneous satisfaction (equality) of all similarity criteria (Reynolds and Froude) is possible only in scale 1:1. Froude similitude in scales smaller than 1 is possible when the viscous forces are negligible (gravity wave). In a short scale model, viscous forces are unimportant compared to gravity and inertia, so it is governed by the Froude similitude (wave propagation). Boundary layer effects are also unimportant.

For a geometrically similar model scaled according to Froude criterion, different scales for friction, surface tension, and elasticity forces are required (Hughes 1993) that are shown in table 1.1 below.

Table 1.1: The scales required to achieve similarity between the prototype and the model. Source: Schüttrumpf 2001

Force	Similitude law	Scale		
		1:1	1:10	1:100
Gravity forces	FROUDE	1	1	1
Friction forces	REYNOLDS	1	1:31.6	1:1000
Elasticity forces	CAUCHY	1	1:10	1:31.6
Capilarity forces	WEBER	1	1:100	1:10000

The critical limits for the influence of viscosity and surface tension for wave propagation are given in the following table (1.2).

Table 1.2: Thresholds (critical limits) established when the effects can be negligible (Schüttrumpf 2001).

Relevant forces	Similitude law	Critical limits
Friction	Fr_w	t>0.35sec
Viscous	Re_w	d>0.2cm
Surface tension	We	$Re_w > Re_{criti} = 10^4$

Where:

$$Fr_w = c/\sqrt{gd}$$

$$Re_w = c*d/\nu$$

$$We = v_A * h_A * \rho_w / \sigma_w$$

c = wave celerity, g= acceleration due to gravity, d= water depth, v_A= wave run-up velocity; h_A = layer thickness at Shallow Water Level.

Bottom and sidewall friction along with internal friction will also result in energy dissipation. For at least 90% of the coastal engineering problems the forces associated with surface tension and elastic compression are small and can be neglected (Warnock 1950). For that reason the Froude and Reynolds number are important as the similarity of one of them along with the geometric similarity, provides the conditions for hydrodynamic similitude of the model (Hughes 1993).

As the model scale decreases, it is difficult to scale down the fluid properties. Small-scale models are expensive to operate, as it is difficult to carry out reliable measurements and so micro modeling is vulnerable to scale effects. For that reason, when using micro models for wave studies, the limitations have to be assessed. Understanding the laboratory and scale effects, improving the similarity criteria, using better instrumentation, automation of the model operation, the models can be utilized to address the problems (Martins 1989).

1.5 Scale effects and micro models

'The model is valid only when the measured quantities in the model are related to their counterparts in the prototype by the ratios that satisfy the similitude criteria' Yalin (1971). The differences between micro modeling and prototype are believed to be the cause of uncertainty in prototype data and the large relaxations in similitude. Micro models were criticized for their accuracy due to their small size.
To begin with, Maynord in his report (2006) criticized the use of micro modeling for river simulation, as the sediment movement is a complex problem having many variables, which are impossible to be reproduced in such a small scale.

Falvey (1999) stated that micro modeling couldn't be used for serious engineering investigations, while Yalin, an expert in movable bed modeling, regrets that micro model cannot be used for predicting purposes. Maynord believes that the previous critics were raised by the micro models' small size and lack of adherence to similarity principles used in movable bed modeling. The proper evaluation parameter is the comparison of bathymetric and flow features to the prototype.

According to Maynord 2006, micro modeling has a small size and large deviations from similarity considerations, and is neither an empirical nor a rational model. It has a large vertical scale distortion, large Froude number exaggeration (velocities 2.7-3.7 times larger than Froude scaling) and not correspondence of stage in model and prototype, so it is placed in a category by itself! Maynord ends up stating the lack of predicting capability by the micro model for movable bed and that the use should be limited to demonstration, education and communication and not for studies where human lives and projects are at risk. It has to be noted that USACE favors the use of micro models, except when human life is on risk. He proposed the following uses:

1. Demonstration of river engineering screening concepts (effects of structures in the rivers), education and communication.
2. Screening tool for: dredging, maintenance and alignments of navigation channels, river modifications and navigation problems around structures.

For movable bed models, Ettema (2001) presents the parameters that influence the flow of water and segment in channels. The last term in his equation is: $\sigma/\rho*g*i*R^2$ (where: σ is the surface tension, ρ is the liquid density, i is the bed slope, R is the hydraulic radius), will not be the same for the prototype and the model, but the effects of differences in

surface tension are negligible. Then it has to be examined if surface tension is negligible in micro models. He also reported that surface tension and viscosity is greater in the laboratory than in reality.

Ettema and Maynord (2002) reported that micro models include all the scale effects, such as large length scales, model distortion, amplification of channel flow and improper sediment size and that the ratio inertia/gravity force is distorted.

Ettema and Muste (2004) concluded that micro models have vertical distortion and is not clear if they can be used to simulate the alluvial channel processes, especially around hydraulic structures.

Beckett (1992) states the sources of scale effects in small-scale tidal models: the lack of turbulent similarity, the sediment size, and the vertical distortion, and surface tension and viscosity effects. He suggested that the minimum water depth must be about 20mm and the horizontal - vertical distortion smaller than 6 (scales 1:1500 and 1:250).

In the current project, the sediment transport is not considered (no movable bed situation) and so micro models can be examined in terms of wave propagation and diffraction, when the scale effects are small and can be negligible. In this occasion, it is believed that micro models can reproduce nature.

1.6 Particle Image Velocimetry (PIV)

For studies taking place some years ago wave probes were used for flow measurements. These measurements were point measurements and nowadays are replaced as they have the following drawbacks:

1. The wave field is incomplete because the measurements cover a small amount of the area.
2. Probes may be located on wrong points (not critical), or can measure additional local effects such as standing waves.

Particle Image Velocimetry (PIV) is a new non-intrusive procedure; an optical measurement technique for the instantaneous mapping of flow fields; quantifying unsteady flow fields (Gray & Greated 1988). It is a method of measuring the velocity vector field of a fluid flow over a given spatial region all at once. It is a quantitative 2D

'snapshot' of the spatial variations in velocity at a point in time (Hughes 1993). Such a multi-point measurement technique is necessary in quantifying and qualifying unsteady flows and flows near interfaces because single-point measurements are no longer sufficient (MAE 2007).

The basic principles of Particle Image Velocimetry are described in Gray and Bruce (1995) along with the problems in the implementation and optimization of the measurement system and examples of their use in offshore engineering.

Ettema (1997) briefly describes the principles underlying the PIV and shows how it can be adapted to the use in hydraulic-model studies of ice-movement problems. Specifically, the PIV was used for a hydraulic model study of ice movement through a confluence of two rivers and it could also be used for remote sensing of ice movement on rivers, coastal regions and oceans.

Fujita et al (1998) implemented a video-based LSPIV (Large-Scale Particle Image Velocimetry) in three hydraulic engineering applications: gas-transfer processes downstream a model spillway, ice conveyance through a model river confluence, and flood plain flow in a full-scale river. They resulted that LSPIV is a reliable, flexible, and economically efficient flow diagnostic tool. It can be successfully used to survey, plan, design, hazard warn, operate, and manage in the water-related activities.

Lengricht J. and Schimmels S. (2000) examined the wave induced flow fields to get their distributions both locally and in time and also get some information about turbulence parameters and energy losses. They also investigated the wave-structure interactions and the complex wave motion in real sea states that consists of numerous wave components superposing or decaying. They concluded that the PIV system allows investigating complex flow phenomena and can give information needed.

The 3D topography wave field measurements were first used by Stagonas (2007) to test the ability of micro models to predict the diffraction process. The author indicated the validity of the method when the PIV measurements were compared to the probes' measurements and resulted in an excellent agreement.

According to the previous studies, it is resulted that PIV can be a powerful tool when mapping the surface flow velocities and is able to replace all the existing old methods.

1.7 Numerical models

Numerical model is a mathematical representation of a physical system. They are mathematical models in which the governing equations are discredited and solved using the computer (Hughes 1993).

In the current thesis Mike 21 Boussinesq model (BW) by DHI will be used to simulate the diffraction phenomenon. According to DHI, Mike 21 BW is the state-of-the-art numerical modeling toll for studies and analysis of wave disturbance in ports and coastal areas. It is an irreplaceable tool for professional coastal engineers and is successfully used for the analysis of operational and design conditions within ports. The software can reproduce the combined effects of all the important wave phenomena of interest in port and coastal areas such as shoaling, refraction and diffraction.

The Mike 21 BW software is based on the numerical solution of the time domain formulations of Boussinesq type equations Madsen et al (1991,1992,1997), Sornsen (2001, 2004). The 2DH BW (two horizontal space co-ordinates) wave model can present wave transformation in coastal areas where the water wave diffraction is important. The 2DH module solves the enhanced Boussinesq equations by an implicit finite difference technique with variables defined on a space-staggered rectangular grid.

2. Methodology

The diffraction coefficient is an expression of the disturbance level at a point inside a port. The determination of the coefficient is of crucial importance, as the engineers have the goal to design a useful structure (port). In this chapter the diffraction coefficient will be calculated using the following three different methods:

1. The micro modeling experimental solution as first introduced by Stagonas (2010).
2. The theoretical solution of Penny and Price (1944).
3. The numerical solution using Mike 21 BW (by DHI)

2.1 The experimental solution using micro models

Stagonas (2010) was the first to examine the water wave diffraction and propagation while using micro models. His experiment is illustrated in the following figure (2.1). The experimental value of the wave height was in a good agreement with the theoretical (linear wave theory) one. The data for the current thesis are the videos of Stagonas' experiment and were provided by him.

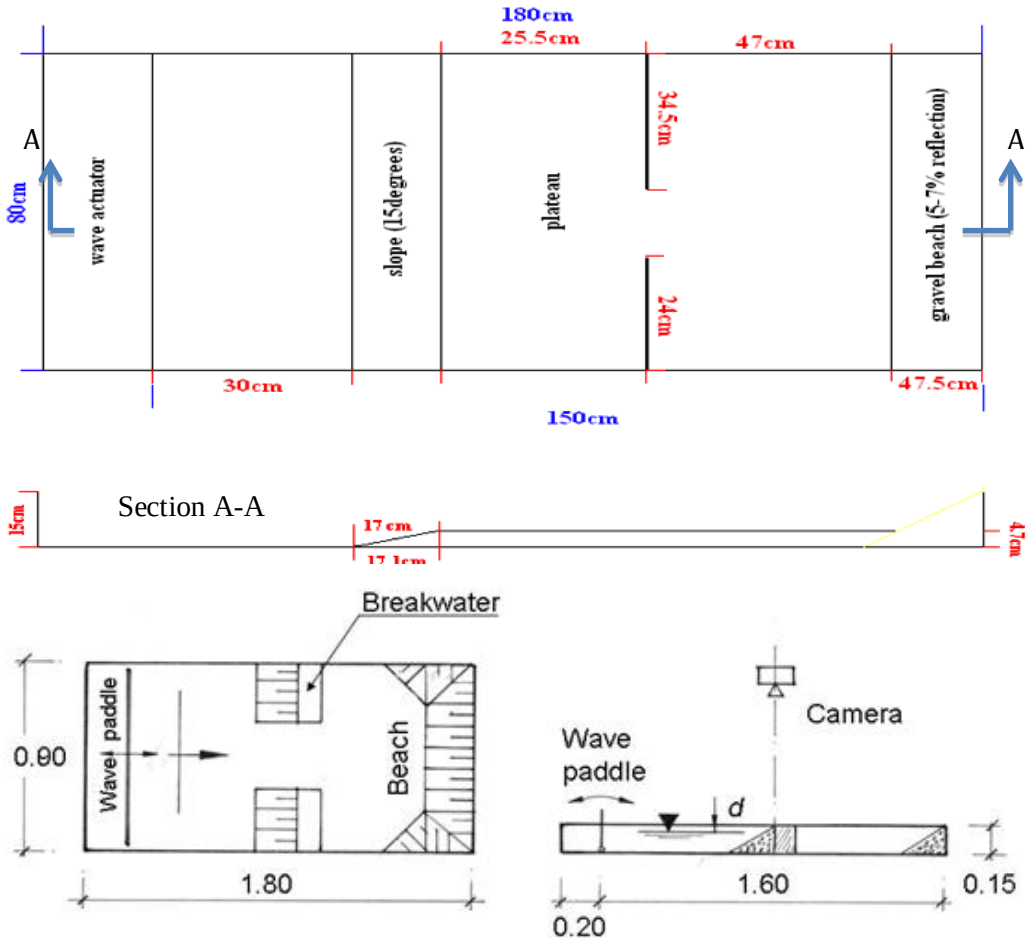

Figure 2.1: The basin's dimensions. Source: Stagonas 2010.

2.1.1 Wave field mapping with Particle Image Velocimetry (PIV)

According to Stagonas' experiment, buoyant tracer particles are seeded in the water and are illuminated with a sheet of pulsed laser light. While the particles were flowing, their position and velocity were measured (recorded photographically). The video will show the path that the particle followed and then velocity maps can be developed as follows: The video is cut into grid cells. Following the Cross correlation method (Gray and Bruce 1995), the distance moved by the tracer between two consecutive images is measured. Knowing this distance and the time required to travel, the velocity of the flow in that cell is calculated, for every interrogation area. At the end, the instantaneous velocity field is exported.

The Assumptions made in order to use the PIV method are:

1. The flow field does not change through time.
2. The velocity in each cell is uniform.
3. The particles have the same velocity with the water particles that they are attached to.

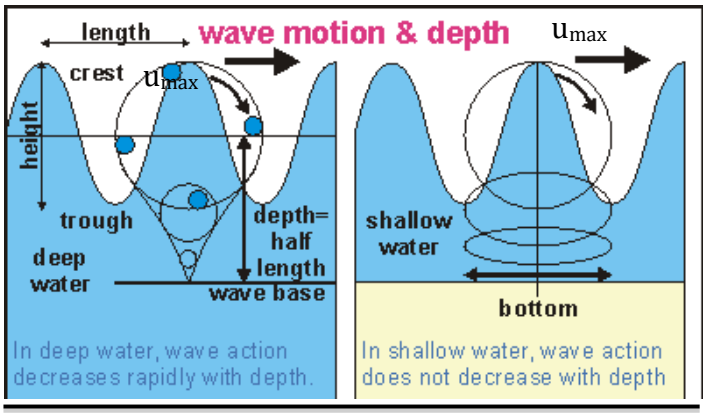

Figure 2.2: The particle motion in deep-water waves.

The maximum horizontal velocity occurs at the surface (figure 2.2) and is calculated according to the linear wave theory as follows:

$$u_{max} = \frac{\pi H}{T} \frac{\cosh\left(k\left(d+\frac{H}{2}\right)\right)}{\sinh\left(kd\right)} \sin\left(\omega t - kx\right) \text{ (Equation 5)}$$

Where:

k = wave number, H = significant wave height, d =water depth, T = wave period and ω = angular frequency.

The surface flow velocities were determined using the Optical flow system VidPIV2.15, a Software that has 32*32 pixel interrogation cells (figure 2.3). The wavelength and period can be calculated using the vector maps provided by the software (figure 2.4).

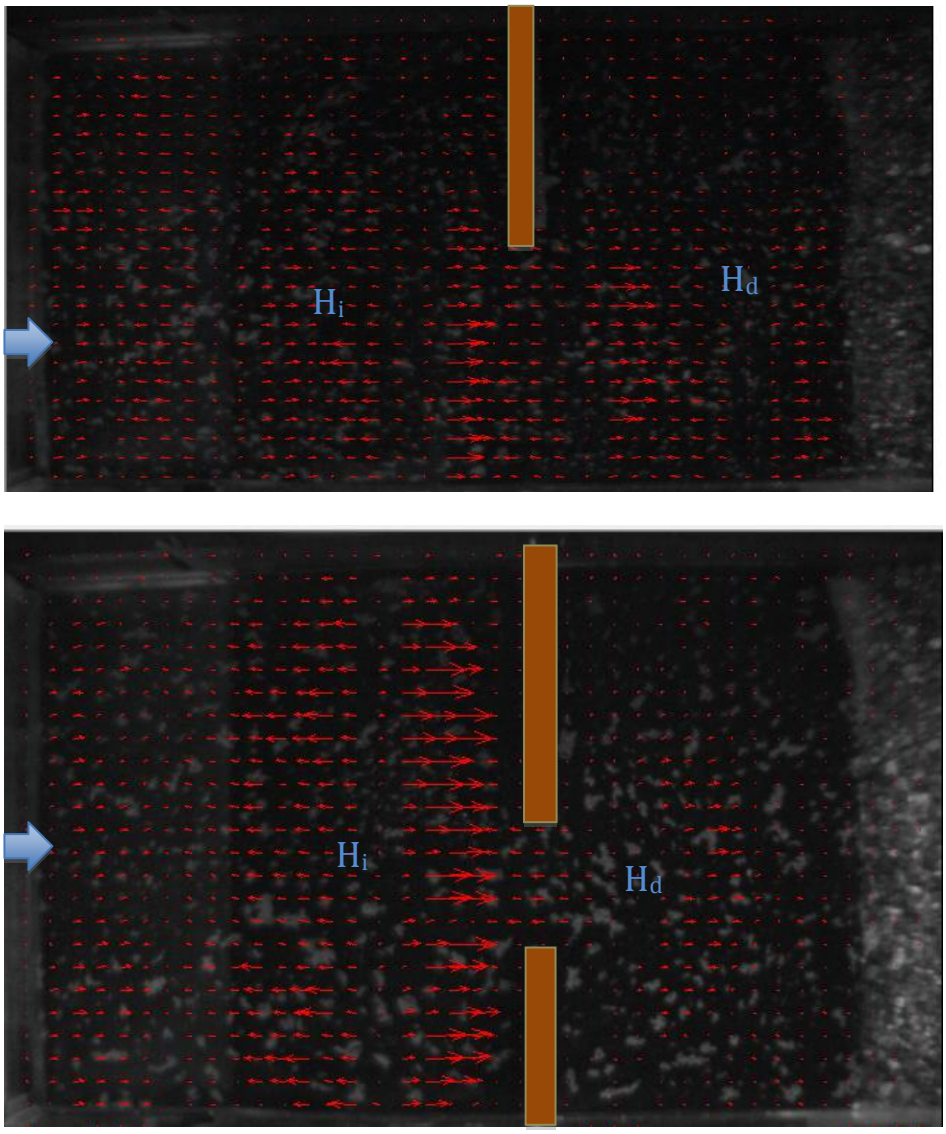

Figure 2.3: The surface flow velocities (velocity vectors in red color) when the wave passes the breakwater or through the breakwater gap.

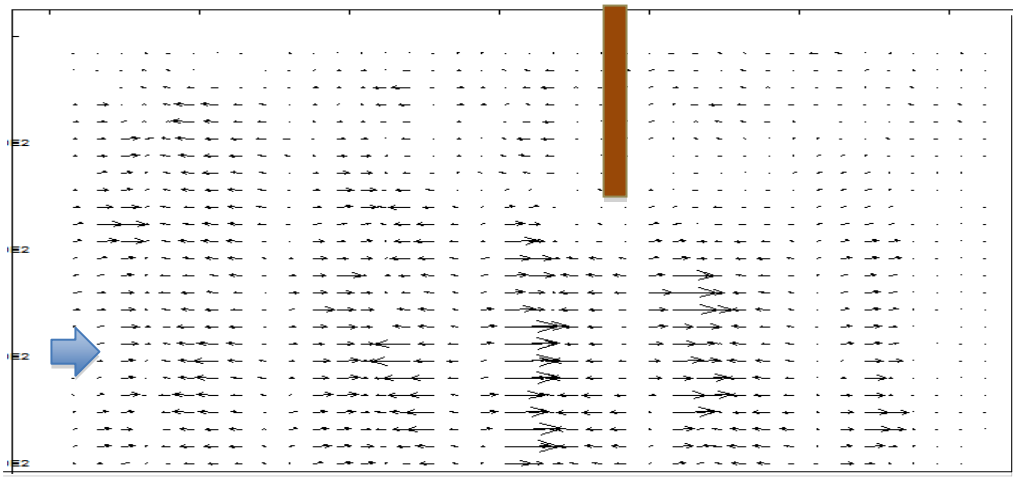

Figure 2.4: The velocity vector maps.

Using the vector map (figure 2.4) the wavelength (L) and the wave period (T) are calculated, as the distance between two consecutive crests (points in figure where the vectors converge) indicates the wavelength. Then using the linear wave theory, the wave period is calculated according to: $L_0=gT^2/2\pi$.

2.1.2 Data

All the information taken by the vector maps is the input on a Matlab script that calculates the incident wave height (H_i) in the basin in the place where no reflection occurs, using the linear wave theory and the Fast Fourier transformation, knowing the water depth and the measured velocities, wavelength and wave period. The incident wave height (H_i) is the average height of all the particles that have the same dimension in the x-axis, just before the breakwater (situated at the plateau; figure 2.1). For more accuracy, the wave height is calculated in the area where the breakwater is absent (figure 2.1), to avoid any reflection caused by the breakwater. The diffracted wave height (H_d) is also calculated at the area just after the breakwater, when the wave had passed the breakwater (knowing that the time between the incident wave height measurement and the diffracted wave height measurement is one wave period). The diffraction coefficient (K') is calculated by dividing those wave heights according to $K'=H_d/H_i$ and can be compared to those extracted by the theoretical and numerical solutions. Having different experiments (videos), using the PIV and Matlab software the following information (wave characteristics) for each one (table 2.1) is exported:

Table 2.1: The wave characteristics of every experiment.

	d_{deep} (mm)	$d_{plateau}$ (mm)	Hi (cm)	L (m)	T (sec)
Exp 4 single breakwater	65	21	0.33	0.16	0.32
Exp 5 single breakwater	65	21	0.65	0.25	0.40
Exp 1 single breakwater	70	26	0.67	0.31	0.44
Exp 2 single breakwater	70	26	0.54	0.21	0.38
Exp 4 breakwater gap	70	26	0.60	0.15	0.32
Exp 5 breakwater gap	70	26	0.60	0.2	0.36
Exp 3 breakwater gap	75	31	0.33	0.16	0.32
Exp 1 breakwater gap	75	31	0.45	0.38	0.49

2.1.3 Superposition of waves

When the wave meets the breakwater is reflected and so a new wave having the opposite direction from the incident is developed. The presence of reflection in the basin causes errors when calculating the wave height without taking the reflection into account, as it increases the wave height in front of the breakwater. In order to present accurately the wave field, the reflected wave has to be considered.

For that reason the Superposition of waves is applied. It is assumed that the waves have small amplitude and the boundary conditions are linear and homogenous. The surface elevation (n_s), is the sum of the incident and reflected wave. According to Stagonas experiments, the waves were approaching perpendicular to the breakwater and so the two waves had the same period, but travel in opposite directions. The surface elevation for every wave in a fixed point (x) is given:

$$n_1 = a_1 e^{i(\omega t - kx + \delta 1)} = a_1 \cos(\omega t - kx)\ ,\ n_2 = a_2 e^{i(\omega t + kx + \delta 2)} = a_2 \cos(\omega t + kx) \quad \text{(Eq 6)}$$

The sum of those two waves is:

$$n_s = e^{i\omega t} \sum a_n e^{i\varphi' n} = (a_1 - a_2)\cos(\omega t - kx) + 2a_2 cos\omega t cos kx \quad \text{(Equation 7)}$$

Where: n= surface elevation, a= wave amplitude and t= time.

The first term represents the progressive wave having amplitude a_1-a_2 and the second is the linear standing wave, having maximum amplitude of $2a_2$. The Matlab script takes into account the reflection when calculating the wave height in the basin.

2.1.4 Shoaling

As the waves travel in areas of non-constant depth (where the depth varies slowly and the bottom slope is very small that negligible reflection occurs so the wave motion is not affected by it) the have characteristics change. As the wave propagates from one depth to another, the wave height and length changes (shoaling or transformation) while the wave period is always constant. The wave height (H) does not influence the phase velocity (c) or the wavelength (L), so L_1 is specified at the point-depth h_1 (using the ratio h_1/L_1) determined from the tables when knowing h_0/L_0.

The equations of determination of the wave height are exported using the fundamental law that no energy is propagated across the wave orthogonal, neglecting the effect of wind stresses that produce energy.

When $H_1$and h_1 are known for a specific point; then H_2 and h_2 at another point can be

calculated according to (Svendsen 1985):

$$H_2 = H_1(\frac{\tanh k1h1}{\tanh k2h2} * \frac{1+G1}{1+G2})^{0.5} \text{ (Equation 8)}$$

Where: $G = 2kh/\sinh 2kh$

When h_1 is for deep-water conditions the equation is simplified to:

$$H = H_0((\tanh kh(1+G))^{-0.5} \text{ (Equation 9)}$$

The values of G, k and h are for the point under examination.

Using the equation 9 instead of 8 arises some errors that are shown in table 2.2 below:

Table 2.2: The amount of error caused by using equation 9.

h_1/L_1	1/4	1/3	1/2	1
Error %	-8	-4.6	-1	0

2.1.5 Scale effects

Not taking into account scale and model effects while setting up a physical model, means that physical modeling is more an art than a science (Oumeraci 1999). Engineers face the challenge to minimize the scale effects of the physical models to ensure that the results of the model are the same as the prototype (Oumeraci 1984). As it was stated earlier, they are the cause of the inability to scale all the relevant forces of the prototype to the model. Scale effects occur due to surface tension and viscous effects and require the careful model set up and interpretation of the results. The cost of overdesigning or under designing can be huge and has to be avoided, apart from the totally wrong modeling that the scale effects cause. Due to those effects (friction by internal and bottom boundary layer) the wave is attenuated. A **damped wave** is a wave whose amplitude of oscillation decreases with time and eventually going to zero.

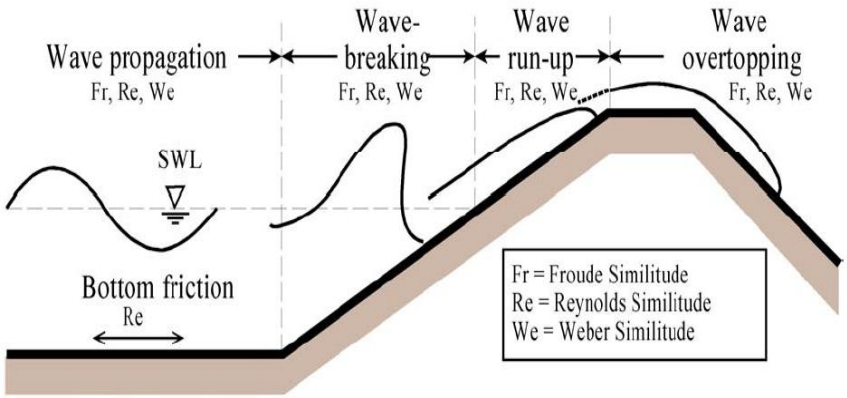

Figure 2.5: The coastal processes and the relevant similitude laws (Schüttrumpf 2001).

Surface tension:

The influence of capillary effects on scale models has to be minimized, as surface tension affects wave celerity and causes wave damping. The influence of surface tension on wave propagation is described by the following equation (Le Mehaute 1976):

$$C^2 = \left[\frac{gL\prime}{2\pi} + \frac{\sigma 2\pi}{\rho L\prime}\right] \tanh \frac{2\pi d}{L\prime} \quad \text{(Equation 10)}$$

The first term presents the gravity and the second is the surface tension (σ).

When σ=0 the wavelength is: $L' = L\left[1 + (\frac{\Delta L}{L})\right]$, and $\frac{\Delta L}{L}$ is a function of the water depth (h or d) and wave period (T).

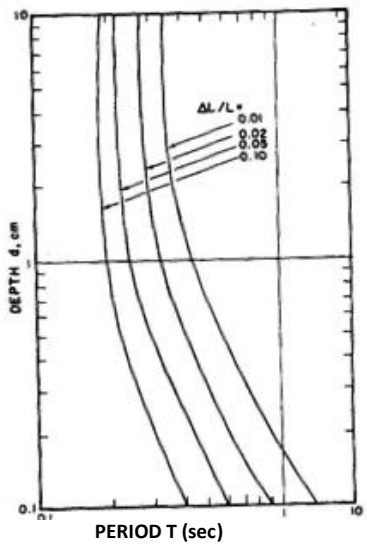

Figure 2.6: The capillary effects (Le Mehaute 1976)

The diagram (figure 2.6) shows that $\frac{\Delta L}{L}$<1% when T>0.35sec and d>2cm. It can be resulted that the depth of 2cm has to be the lower limit for scale models, where viscous damping is negligible (Le Mehaute 1976). The surface tension's effects are important when the waves are short and the water depth is very shallow. Le Mehaute (1976) and Keulegan (1950b) reported that the effect of viscous damping in non-breaking waves travelling in short distances is negligible when d>2cm. Wave height attenuation decreases as the water depth (d), wave period (T) and tank width increases. Stagonas (2010) added to the previous when in his experiments did not observe any wave damping for water depth d>0.04m and T>0.3sec.

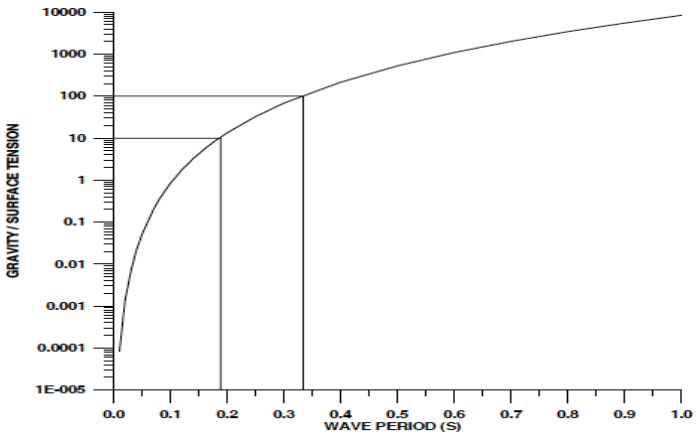

Figure 2.7: The relation between gravity and surface tension of the equation of Tirindelli et al (2000), for different wave periods.

As figure 2.7 above shows, for laboratory waves having T>0.35sec and d>2cm, the surface tension is 100 times smaller than gravity and so surface tension does not affect the waves.

Dong et al (2007) applied the diffraction method to investigate the proprieties of liquid surface. It was observed that the damping constant (a) is increasing with the frequency. Then they compared the diffraction method and two other methods (the imaging analyzer method and the capacitive antenna method) with the theoretical. At the low frequency, all of them could obtain nearly the same results as the theoretical prediction. However, at the higher frequency, the results of the imaging analyzer method became inaccurate, whereas, the diffraction method and the capacitive antenna method can still get the accurate results for the liquid surface wave (LSW) damping problem at a few hundreds hertz.

It was noted that the surface wave attenuation depends upon the wave frequency. The amplitude is assumed to be much smaller than the wavelength. The spatial damping constant of the surface wave is approximately given by the hydrodynamics' theory as:

$$a = \frac{8}{3}\frac{\pi \nu \rho f}{\sigma},$$

Where:

$\sigma =$ Surface tension, ϱ = the density of the sample liquid, and ν= kinetic viscosity= μ/ρ, f = the LSW frequency.

For pure water at 25°C: $\nu = 0.897 * 10^{-6} m^2/s$, ρ = 997,1kg/m^3, σ =7, 26 10 $^{-2}$ N/m

The relationship between the wave amplitude (h) and the distance (x) is:

$$h = h_0 e^{(-ax)} \quad \text{(Equation 11)}$$

Viscosity:

The influence of viscosity to wave propagation (on wave celerity) is given by Biesel (1949):

$$c = \left\{1 - \frac{1}{\sinh\left(\frac{4\pi d}{L}\right) * \sqrt[4]{\frac{gL^3}{2\pi^3\nu^2}\tanh\left(\frac{2\pi d}{L}\right)}}\right\}\sqrt{\frac{gL}{2\pi}\tanh\left(\frac{2\pi d}{L}\right)} \quad \text{(Equation 12)}$$

Where: c= wave celerity, d = water depth, ν = viscosity and L = wavelength.

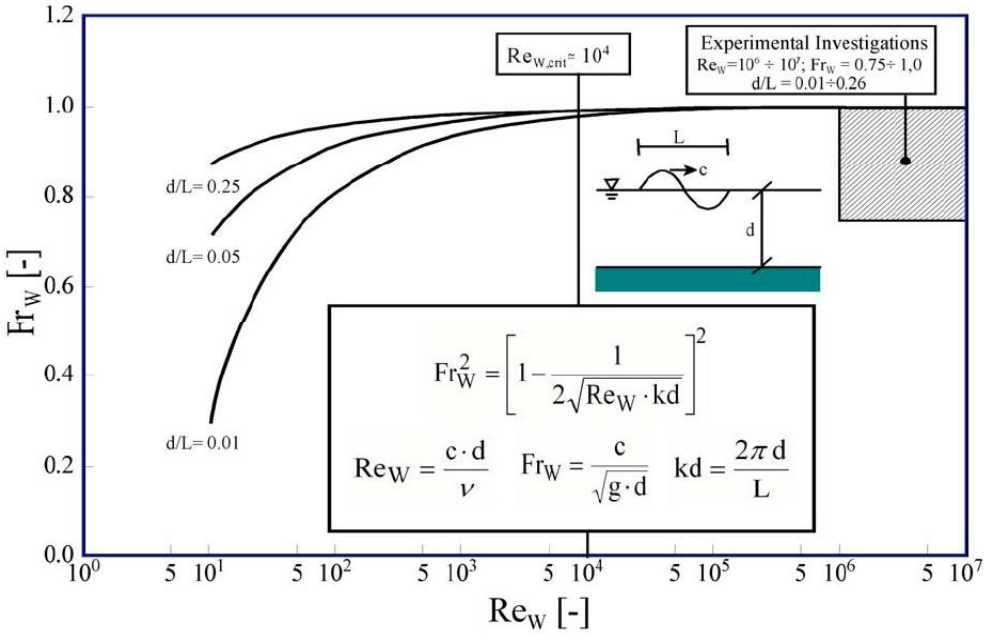

Figure 2.8: The influence of viscosity on wave propagation (Schüttrumpf2001)

Figure 2.8 describes the influence of viscosity (by a wave Reynolds-number (Rew)) on wave propagation (given by a wave Froude-number (Frw)). The influence of viscosity is negligible for wave Reynolds number less than 10^4.

When scaling according to Froude criterion, the viscous and friction effects are not simulated, as the Reynolds number in the model is different than in the prototype. Keulegan (1950a) estimated the wave height attenuation because of the **internal friction:**

$$\frac{d}{dt}\left(\pi\rho\frac{H^2C^2}{4L}\right) = -16\pi^3\rho\nu\frac{H^2C^2}{4L^3} \quad \text{(Equation 13)}$$

The left side represents the time rate of change of wave energy per unit surface area in a linear wave, while the right side is the average rate of energy conversion per unit area due to internal shearing stresses.

By rearranging and integrating the equation becomes:

$$\frac{H(t)}{H_{t=0}} = e^{-(\frac{8\pi^2 \nu t}{L^2})} \quad \text{(Equation 14)}$$

Where: H (t) is the attenuated wave height at the time t, ν = viscosity=1,4*10^{-6} m^2/sec.

The equation can be used for uniform regular waves travelling on a horizontal bed. Because of the thin boundary layer, internal friction is minimal and dissipation of energy due to viscous for non-breaking waves travelling in a short distance is limited (Hughes 1993). Kaulegan (1950b) estimates the wave attenuation of regular waves in a rectangular channel with uniform and constant cross section:

$$\frac{H_2}{H_1} = e^{-\alpha x_p} \quad \text{(Equation 15)}$$

Where: $\alpha = \frac{2}{bc}\sqrt{\frac{\pi\nu}{T}}\left[\frac{\sinh(\frac{4\pi h}{L})+\frac{2\pi B}{L}}{\sinh(\frac{4\pi h}{L})+\frac{4\pi h}{L}}\right]$

x_p= the horizontal distance in flume, H_1= wave height at x_p=0, H_2= wave height at x_p,
b= width of the tank, c= wave celerity, L=wavelength, h= water depth,
T= wave period and ν = kinematic viscosity.

The wave attenuation due to **sidewall and bottom friction** is given by (Hunt 1952):

$$\frac{\frac{dH}{dx}}{H} = -\frac{2k}{d}\frac{\sqrt{\upsilon}}{\sqrt{2\omega}}\left(1+\frac{2kd}{sinh\,2kd}\right)^{-1}\left(\frac{2kd}{sinh\,2kd}+\frac{2d}{b}\right) \quad \text{(Equation 16)}$$

Where: b= width of the tank

The equations above (11,15 and 16) are applied in order to get the wave damping in the experimental basin.

2.2 The theoretical solution of diffraction

Penny and Price (1944) showed that Somerfield's (1986) solution of the optical diffraction could be also the solution for water wave diffraction problem.

2.2.1 Diffraction around a Single breakwater:

Since the surface elevation is known for every point within the basin (using the PIV), the value of the diffraction coefficient can be calculated at a given position.

When waves travel towards the breakwater having an incident angle θ with the breakwater, are diffracted. Having a specific point where the diffracted wave height and diffraction coefficient are measured, the distance from the breakwater tip (r) (figure 2.9) and the angle θ_o or β are the input parameters in the following equations.

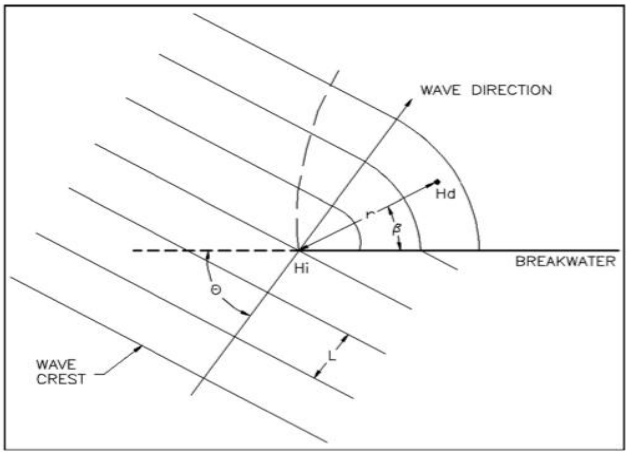

Figure 2.9: The characteristics of the wave diffraction phenomenon.

A Fortran script was developed by Karambas (Professor of Aristotelio University of Thessaloniki), using the equations of Penny and Price (1944) shown below, to calculate the wave attenuation (diffraction coefficient) due to the diffraction by a single breakwater.

The diffraction coefficient is calculated by the modulus of F (r,θ):

$$K' = |F(r,\theta)| \text{ (Equation 17)}$$

Where:

$$F(r,\theta) = exp\{-ikrcos(\theta - \theta o)\} * f(\sigma) \pm exp\{-ikrcos(\theta - \theta o)\} * f(\sigma')$$

$$\sigma = 2 * \sqrt{\frac{kr}{\pi}} * sin\frac{1}{2}(\theta - \theta o)$$

$$\sigma' = -2 * \sqrt{\frac{kr}{\pi}} * sin\frac{1}{2}(\theta + \theta o)$$

and

$$f(\sigma) = 0.5 * [(1 + C + S) - i(S - C)]$$

$$f(-\sigma) = 0.5 * [(1 - C - S) + i(S - C)]$$

Where:

k = wave number , θ = incident wave propagation angle, θo = the angle formed between the edge of the breakwater and r, or else the deviation angle.

C, S: are the Fresnel integrals, which can be replaced by the polynomial approximations (Kim and Lee (2009)).

In this project the waves approach the breakwater perpendicular, at an angle of 90° (the incident angle (θ) is 90° degrees) and the angle between the point of measurement and the breakwater (θ_o or β) can be 45° or 90° or 135° as figure 2.10. Table 2.3 gives the theoretical values of the diffraction coefficient.

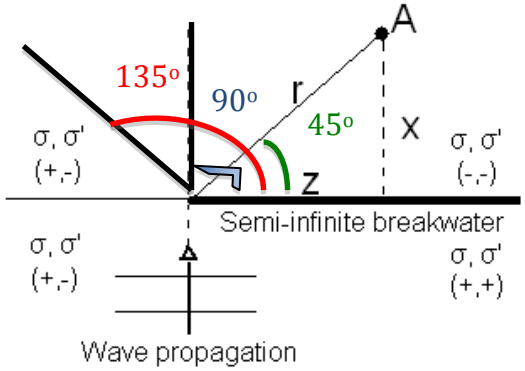

Figure 2.10: Nomenclature for wave diffraction analysis at breakwater tip (Wiegel 1976).

Table 2.3: The diffraction coefficient (K') as a function of the incident wave angle (90°), position (r/L) and θ_o. Source: Wiegel 1962.

r/L	θ_o or β (degrees)		
	45°	**90°**	**135°**
0.5	0.96	0.59	0.36
1	1.07	0.56	0.28
2	1.04	0.54	0.2
5	1.05	0.53	0.13
10	0.96	0.52	0.09

2.2.2 Diffraction of waves passing through a Breakwater gap

Both tips of the breakwater affect the wave height at any point where the waves had passed the breakwater. The theory used, was first developed by Penny and Price (1944, 1952) where the diffraction coefficient is given by:

$$K' = |F\,(r, \theta)|$$

Figure 2.11 illustrates the factors that are used to solve the following equations.

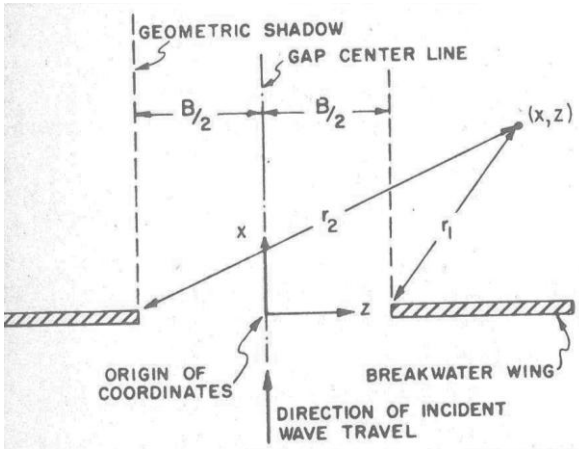

Figure 2.11: Nomenclature for breakwater gap problem. Source: Blue and Johnson (1949).

The solution of F equals the following for the five different regions:

$-f_1+g_1$		f_1+g_1
$+f_2+g_2$		$-f_2+g_2$
	e^{-iky}	
	$-f_1+g_1$	
rigid breakwater	$-f_2+g_2$	rigid breakwater
$e^{-iky}+e^{iky}$		$e^{-iky}+e^{iky}$
$-f_1+g_1$		$-f_1-g_1$
$-f_2-g_2$		$-f_2+g_2$

Where:

$$f_1 = e^{-ikx} f\,(-\sigma_1)$$
$$f_2 = e^{-ikx} f(-\sigma_2)$$
$$g_1 = e^{-ikx} f(-\sigma'_1)$$
$$g_2 = e^{-ikx} f(-\sigma'_2)$$

$$\sigma_1 = -\sqrt{\frac{4(r_1 - x)}{L}},\ \sigma'_1 = -\sqrt{\frac{4(r_1 + x)}{L}},$$

$$\sigma_2 = -\sqrt{\frac{4(r_2 - x)}{L}},\quad \sigma'_2 = -\sqrt{\frac{4(r_2 + x)}{L}}$$

Where: r = straight distance from the breakwater, B = the breakwater gap, x = perpendicular distance from the breakwater, z = horizontal distance from the breakwater. In this project the breakwater gap is B=21,5cm and the wavelength (L) varies from 15cm to 31 cm. The experimental values of x/L are up to 2 and for y/L are up to 2.5, covering the small area of the graphs (B/L~1 and B/L~1.41), as illustrated in red colour in figure 2.12 below.

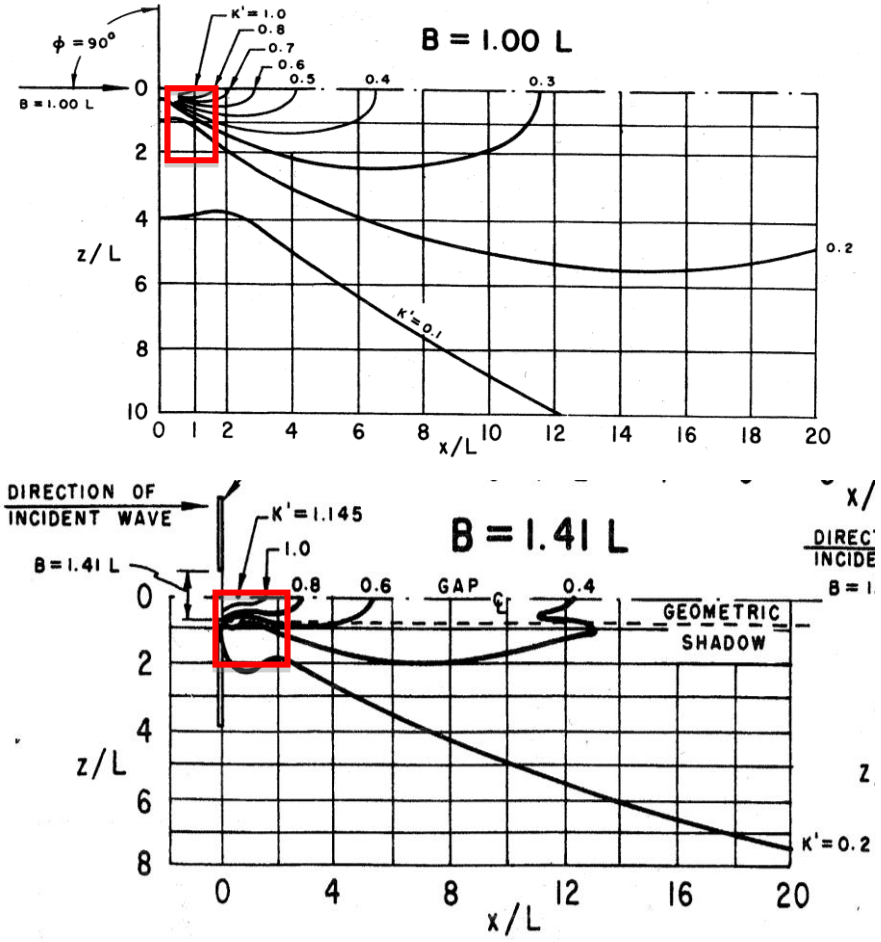

Figure 2.12: The theoretical contours of equal diffraction coefficient at a breakwater gap for B/L=1 (top) and 1.41 (down) (Johnson 1952).

Contour plots of the diffraction coefficient will be developed in that small area just after the breakwater.

2.3 The numerical solution- Mike 21 (by DHI)

The purpose of using this software is to illustrate the diffraction phenomenon, taking place in the experimental basin.

Due to the small dimensions of the basin and values of the wave characteristics, the model was scaled up. The Hydraulic processes in prototype can only be transferred to model scale if the similarities are fulfilled simultaneously. The geometrical similarity is fulfilled by a constant ratio ($1/N_L$) between all lengths in prototype and model, in this occasion 1/100. The fulfillment of the kinematical similarity requires identical time intervals for geometrical similar distances in prototype and model scale and is fulfilled by reducing all time intervals by $1/(N_L)^{0.5}$, according to Froude law.

Using Mike 21 BW setup planner, all the data such as time step and spatial resolution are provided. The grid spacing depends on the water depth, so is different each time (the values vary between 1.2-1.8m). The time step also varies depending on the wave period. The simulation period is chosen to be 60 sec, which is the time that the video lasts, corresponding to the number of time steps according to: 60* simulation time/ time step = number of time steps.

The model setup is illustrated in figure 2.13 for the single breakwater and the breakwater gap. The size of the basin is 34m by 80m with a uniform depth of 3.11m, 2.61m and 2.11m in the shallow area in front of the breakwater. Wave absorbing sponge layers are applied at the model boundaries to prevent waves being bounced back into the domain, and their thickness is about one times the wavelength. The area of interest is the shadow zone behind the breakwater. Due to radiation of energy from the point of diffraction, the western boundary has to be placed quite far from this area to avoid reflections. Internal wave generation is applied as open boundaries are fully reflective and will therefore reflect any wave energy radiating out of the model area back into the model. A sponge layer behind the wave generation line is used to absorb waves heading out of the domain from the generation line to avoid reflections.

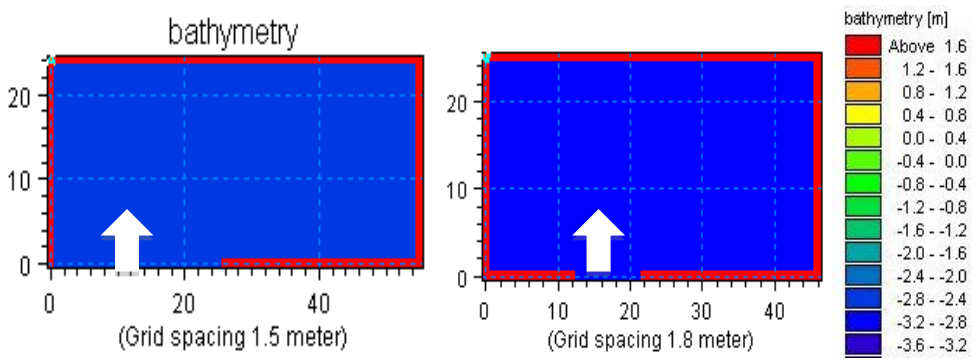

Figure 2.13: The model layout: single breakwater (left), breakwater gap (right).

3. Results & Discussion

3.1 Single breakwater

3.1.1 The theoretical solution

The Penny and Price solution for a single breakwater gives the following diffraction coefficient (table 3.1) having different water depth (d), wave length (L) and period (T) for each experiment:

Table 3.1: The theoretical diffraction coefficient (K') for different positions in the basin (see figure 2.10).

- For T=0.44 sec and water depth= 26mm, L=0.31m (exp1).

r (m)	θ=90°	r (m)	θ=45°	θ=135°
0.16	0.57	0.18	0.29	1.01
0.19	0.56	0.22	0.31	1.09
0.22	0.56	0.27	0.24	1.04
0.25	0.55	0.31	0.23	0.97
0.28	0.55	0.36	0.21	*

- For T=0.38 sec and water depth=26mm, L=0.21m (exp 2).

r (m)	θ=90°	r (m)	θ=45°	θ=135°
0.16	0.561	0.18	0.268	1.082
0.19	0.557	0.22	0.246	1.095
0.22	0.553	0.27	0.228	1.089
0.25	0.549	0.31	0.211	1.059
0.28	0.546	0.36	0.199	*

- For T=0.32 sec and water depth= 21mm L=0.16m (exp 4).

r (m)	θ=90°	r (m)	θ=45°	θ=135°
0.16	0.553	0.18	0.236	1.094
0.19	0.548	0.22	0.216	1.069
0.22	0.545	0.27	0.199	1.026
0.25	0.542	0.31	0.183	0.968
0.28	0.539	0.36	0.1734	*

- For T=0.4 sec and water depth= 21mm, L=0.21m (exp 5).

r (m)	θ=90°	r (m)	θ=45 °	θ=135°
0.16	0.562	0.18	0.266	1.084
0.19	0.556	0.22	0.244	1.095
0.22	0.552	0.27	0.227	1.087
0.25	0.549	0.31	0.209	1.056
0.28	0.546	0.36	0.198	*

The value that is missing at the end of the table (*) is out of the grid/range.

3.1.2 Micro modeling

The outputs of the PIV and Matlab were plotted (using 'Surfer 10' software) and shown in the figures below (3.1 and 3.2):

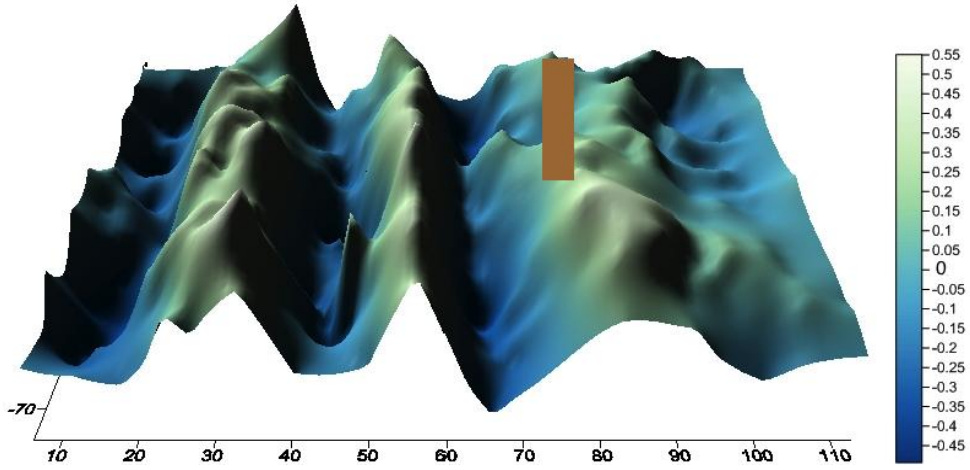

Figure 3.1: The wave propagating in the basin, interrupted by a single breakwater. Wave characteristics: T=0.4sec, L= 0.25m, d_{deep}=65mm and Hi=0.65cm (file name: run5sbwd65)

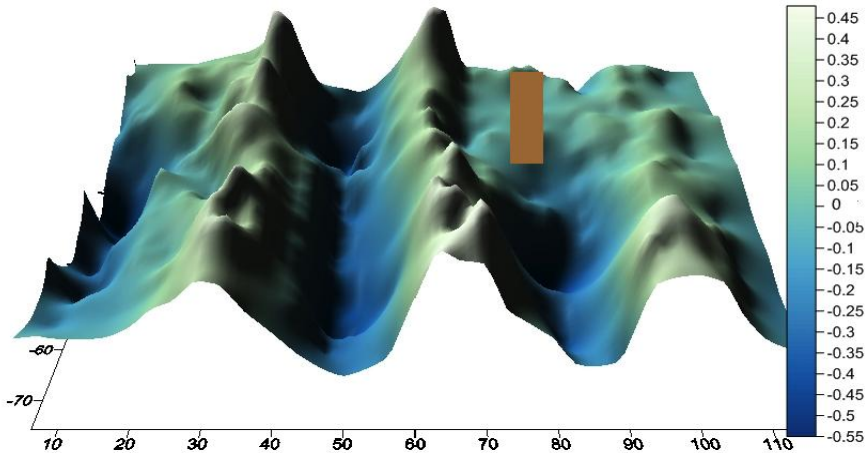

Figure 3.2: The wave propagating in the basin, interrupted by a single breakwater. Wave characteristics: T=0.44sec, L= 0.31m, d_{deep}=70mm and Hi=0.67cm (file name: run1sbwd70)

The figures 3.1 and 3.2 above illustrate the 3D wave field in the experimental basin. As it can be seen, no wave height reduction occurs between the 'open sea' and the un-sheltered area after the breakwater. In contrast, the wave height is reduced on the lee of the breakwater having a rate that increases as the distance from the structure increases (in case where two diffracted waves are present in the basin).

The reflections that take place in the edge of the basin (see figure 3.1) create waves that have different direction from that of the incident wave, and increase the wave height after superposition. Due to the small scale, reflection from the breakwater and the side walls and the absence of active absorption, the data couldn't be more accurate as the wave field 'is destroyed' in a few seconds. The scale effects are the reason that reduces the wave height in the basin.

For the same positions in the basin as the theoretical solution, the micro modeling solution is given in table 3.2:

Table 3.2: The experimental (micro modeled) diffraction coefficient.

	d (mm)	**Hi (cm)**	**K' (θ=45°)**	**K' (θ=90°)**	**K' (θ=135°)**
Exp 4 single bw	65	0.33	0.24	0.41	0.75
Exp 5 single bw	65	0.65	0.18	0.70	1.29
Exp 1 single bw	70	0.67	0.23	0.36	1.06
Exp 2 single bw	70	0.54	0.12	0.59	1.43

Table 3.3 below puts together the two solutions.

Table 3.3: The theoretical and experimental (micro modeled) diffraction coefficient (K').

	K_{m-m}' (θ=45°)	**K_{th}' (θ=45°)**	**K_{m-m}' (θ=90°)**	**K_{th}' (θ=90°)**	**K_{m-m}' (θ=135°)**	**K_{th}' (θ=135°)**
Exp 4 single bw	0.24	0.20	0.41	0.54	0.75	1.02
Exp 5 single bw	0.18	0.22	0.70	0.55	1.29	1.08
Exp 1 single bw	0.23	0.24	0.36	0.55	1.06	1.04
Exp 2 single bw	0.12	0.24	0.59	0.55	1.43	1.08

Using the table above it is easy to compare the two solutions. It can be concluded that a good agreement is observed between the micro-model and theory in most of the positions in the basin. The experimental (micro modeled) diffraction coefficient is generally closed to the theoretical one, apart from some positions. In most of the cases the deviation is about 20% apart from the positions near the boundaries where the values of the

coefficient are far from the theory. This is most probably due to the reflections that occur in the basin due to the side walls. For example, figure 3.1 (exp 5) shows that the diffracted wave height at 135^o is large due to the reflection from the side wall, resulting in a bigger value of K' ($=H_d/H_i$) than the theoretical.

Stagonas (2010) believes that the errors affecting the accuracy of wave height (H) in his experiments are the cause of:

1. The velocities in one interrogation area are constant.
2. The low resolution of the camera (1 pixel covers the area of $1.76mm^2$) is large and losses the accuracy.
3. In order to use the linear theory, many simplifying assumptions are made, so the accuracy is limited.

Those errors also affect the current thesis as the data are provided by Stagonas' experiments.

As an overview, it can be concluded that the experimental results about the diffraction of waves around a single breakwater in micro-models are encouraging. Although some differences were observed between the model and theory, those are within the limits suggested in the existed literature.

3.1.3 Mike 21

The numerical results are presented in Figures 3.3-3.5 showing a contour plot of the instantaneous surface elevation and the maps showing the isolines of the wave disturbance coefficient in the entire domain. The modeled area was rotated 90^{o} anti clockwise and the blue vectors show the wave direction.

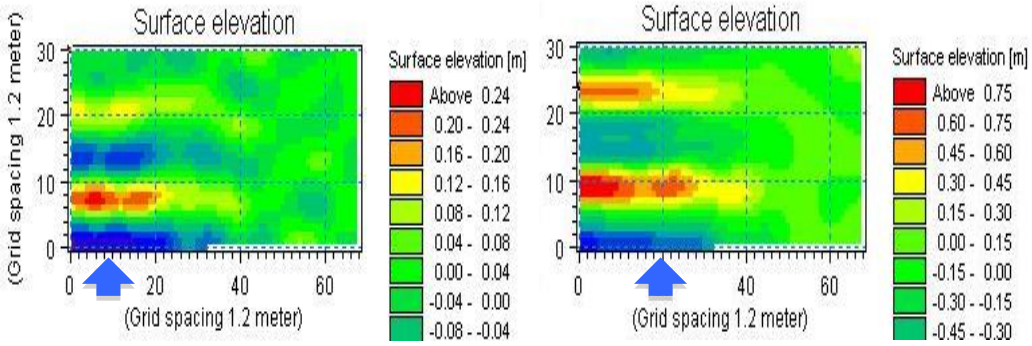

Figure 3.3: The instantaneous surface elevation. Left: exp4; L= 0.16m and right: exp5; L=0.25m (water depth d=0.065m).

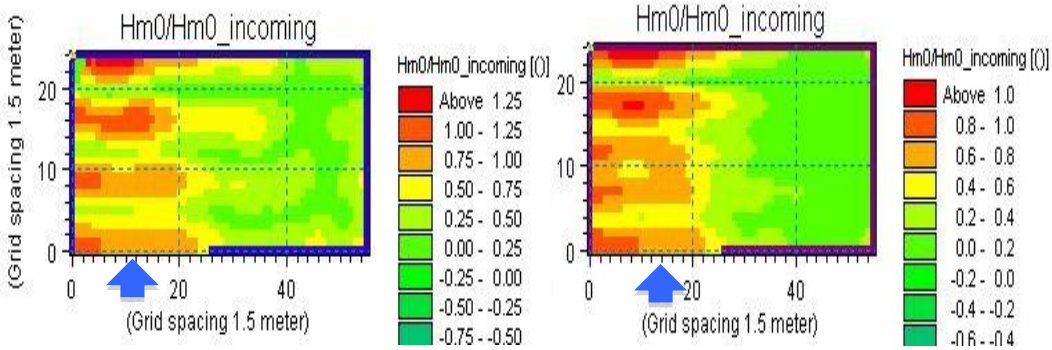

Figure 3.4: The numerical diffraction coefficient ($K'=H_d/H_i$) for a single breakwater. Left: exp1; L= 0.31m and right: exp2; L=0.21m (water depth d=0.07m).

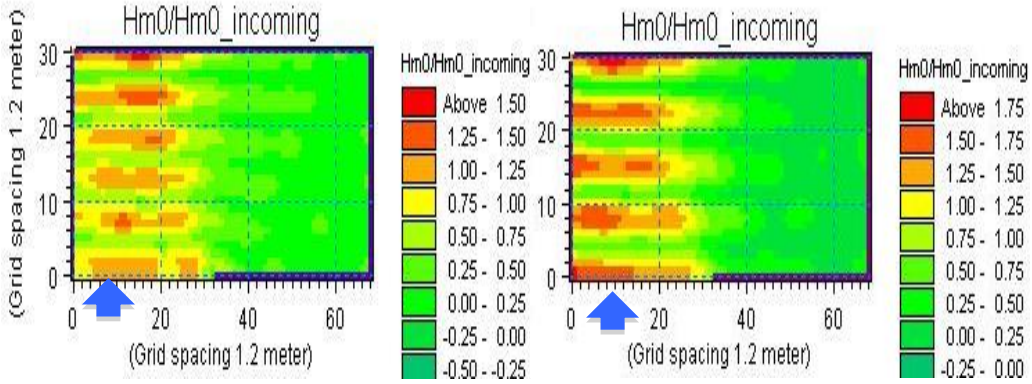

Figure 3.5: The numerical diffraction coefficient ($K'=H_d/H_i$) for a single breakwater. Left: exp4; L= 0.16m and right: exp5; L=0.25m (water depth d=0.065m).

The numerical results for the same positions in the basin as the theoretical ones are given in table 3.4 below.

Table 3.4: The theoretical and numerical diffraction coefficient (K').

	K_{mike21}' (θ=45°)	K_{th}' (θ=45°)	K_{mike21}' (θ=90°)	K_{th}' (θ=90°)	K_{mike21}' (θ=135°)	K_{th}' (θ=135°)
Exp 4 single bw	0.22	0.20	0.54	0.54	1.14	1.02
Exp 5 single bw	0.2	0.22	0.72	0.55	1.5	1.08
Exp 1 single bw	0.4	0.24	0.56	0.55	1	1.04
Exp 2 single bw	0.2	0.24	0.5	0.55	0.83	1.08

As it was predicted, the numerical results are in good agreement with the theoretical ones. Mike 21 as every numerical model, in order to be valid, its results have to be in good agreement with the semi-analytical solutions of Shore Protection Manual (1984). The big values of K' (K'>1, values in red colour in figures 3.4 & 3.5) in some experiments are the cause of reflections due to the side walls - boundaries.

Table 3.5: The theoretical, experimental and numerical values of the diffraction coefficient (K')

EXP 1			**θ=45°**	**θ=90°**	**θ=135°**
L (m)	0.31	Theoretical	0.24	0.55	1.04
d (m)	0.0261	Experimental (m-m)	0.23	0.36	1.06
H(cm)	0.67	Numerical (Mike21)	0.4	0.56	1
T(sec)	0.44				
EXP 2					
L (m)	0.21	Theoretical	0.24	0.55	1.08
d (m)	0.0261	Experimental (m-m)	0.12	0.59	1.43
H(cm)	0.54	Numerical (Mike21)	0.2	0.5	0.83
T(sec)	0.38				
EXP 4					
L (m)	0.16	Theoretical	0.2	0.54	1.02
d (m)	0.0211	Experimental (m-m)	0.24	0.41	0.75
H(cm)	0.33	Numerical (Mike21)	0.22	0.54	1.14
T(sec)	0.32				
EXP 5					
L (m)	0.25	Theoretical	0.22	0.55	1.08
d (m)	0.0211	Experimental (m-m)	0.18	0.7	1.29
H(cm)	0.65	Numerical (Mike21)	0.20	0.72	1.5
T(sec)	0.4				

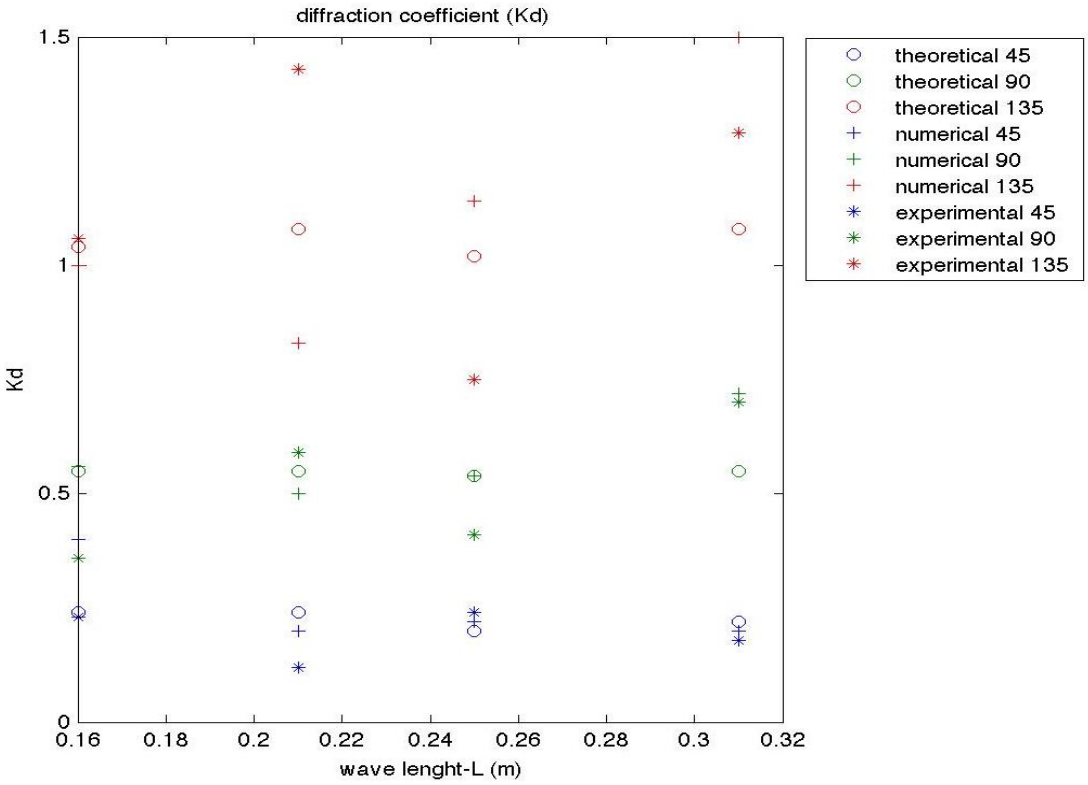

Figure 3.6: The theoretical, experimental and numerical diffraction coefficient in the three positions in the basin for the different wave length.

Table 3.5 summurises the results of the three methods (theoretical, experimental and numerical) to have a better view and be able to compare them. Having four different data series for a single breakwater with different wave length and incident wave height, the theoretical, experimental and numerical diffraction coefficient is calculated. The values of the coefficient are then plotted in figure 3.6 against the wave length. The results are generally in a good agreement appart from some positions in the wave basin which are near the boundaries (side walls) of the basin where reflection occurs that increases the diffracted wave height and results in a bigger value of the diffraction coefficient (K' = H_d/H_i).

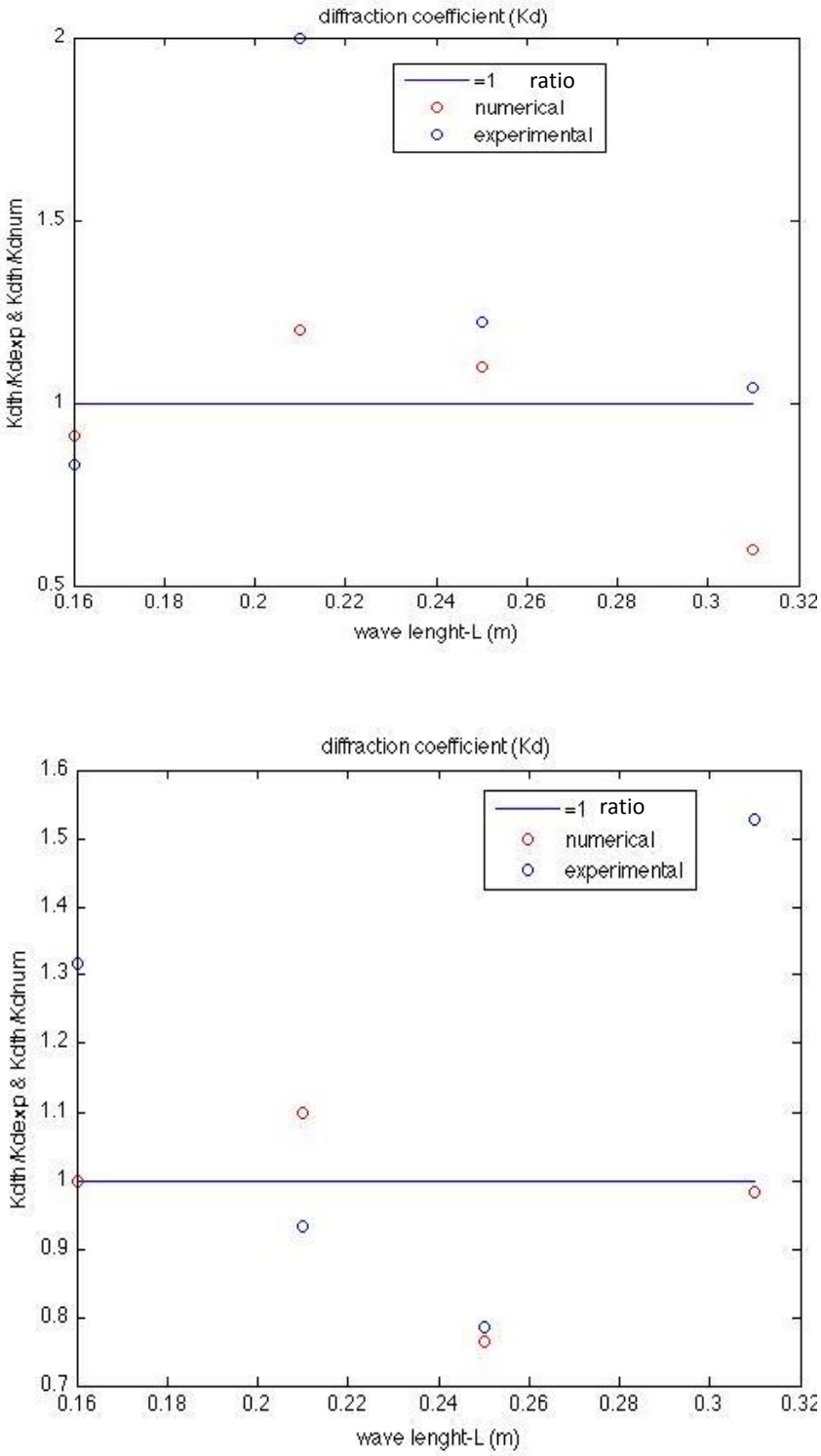

Figure 3.7: The ratio of the theoretical diffraction coefficient to the numerical and experimental, plotted for different wave length, for two positions in the basin; $\vartheta=45^{o}$ (top) and $\vartheta=90^{o}$ (below).

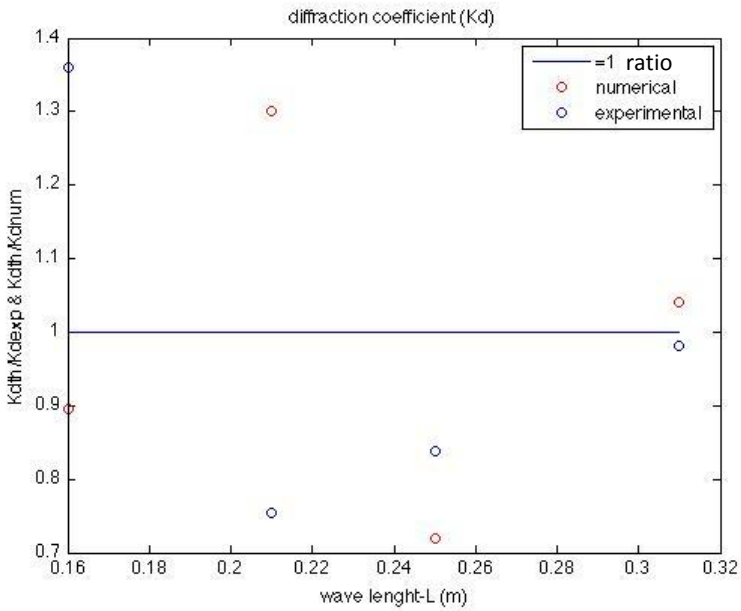

Figure 3.8: The ratio of the theoretical diffraction coefficient to the numerical and experimental, plotted for different wave length, for the position of ; ϑ=135^o in the basin.

As table 3.5 and figures 3.7 & 3.8 above indicate, the values of K' of the three methods are in good agreement. The value of K_{th}/K_{exp}=1 and K_{th}/K_{num}=1 indicates the ideal agreement between the methods. The deviation from unity is expected, but the smaller the better. Any relation between the wavelength and the deviation from unity cannot be exported. This agrees with the literature, as for the values of T>0.35sec and d>0.2cm (thresholds) the scale effects are negligible and do not affect the wave field. The same is concluded in figure 3.9 below, where the wave height doesn't affect the diffraction coefficient.

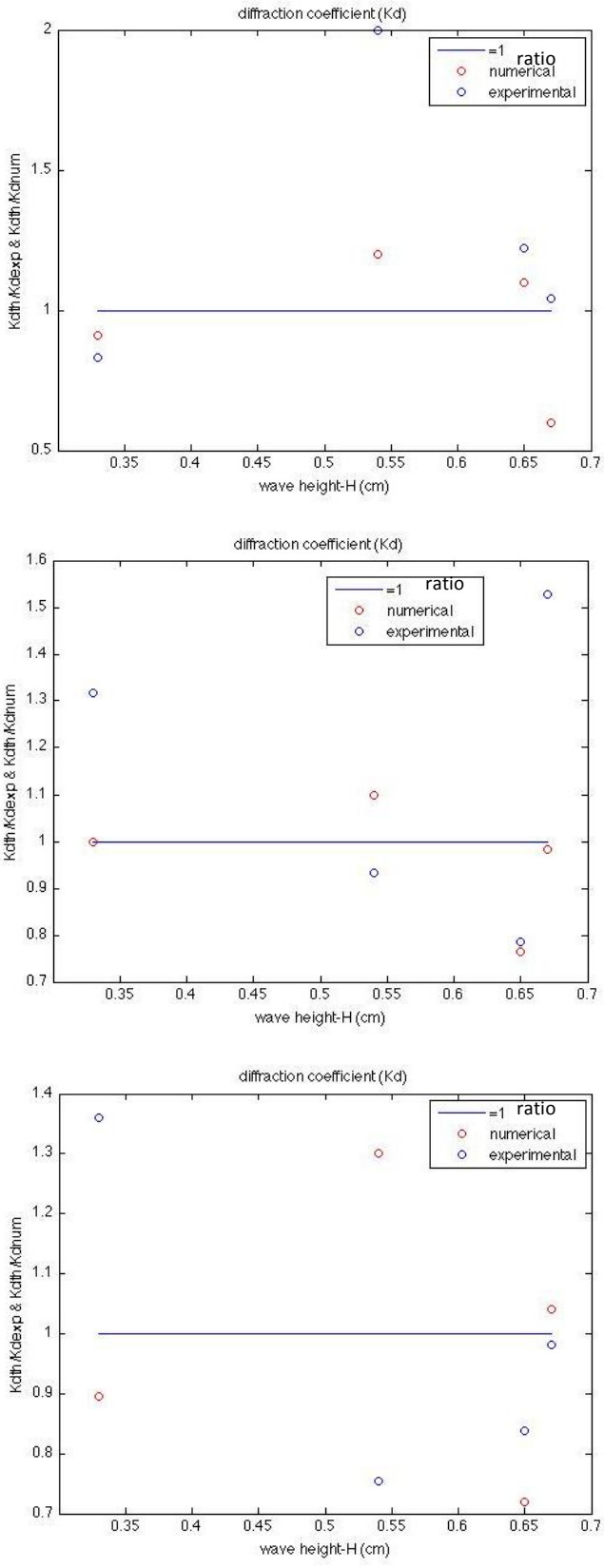

Figure 3.9: The ratio of the theoretical diffraction coefficient to the numerical and experimental, plotted for different wave length, for the three positions in the basin; ϑ=45^o (top), ϑ=90^o (middle) and ϑ=135^o (down) .

3.1.4 Scale effects

Applying the three equations (11,15 and 16; pages 37-41) for the situation where the experimental basin was 1.8*0.8m, the water depth d_0-d=0.07-0.0261m, the wave length L=0.3m, wave period T=0.44sec and the wave height in deep water H_0=0.01m, the following wave attenuation in deep water is resulted:

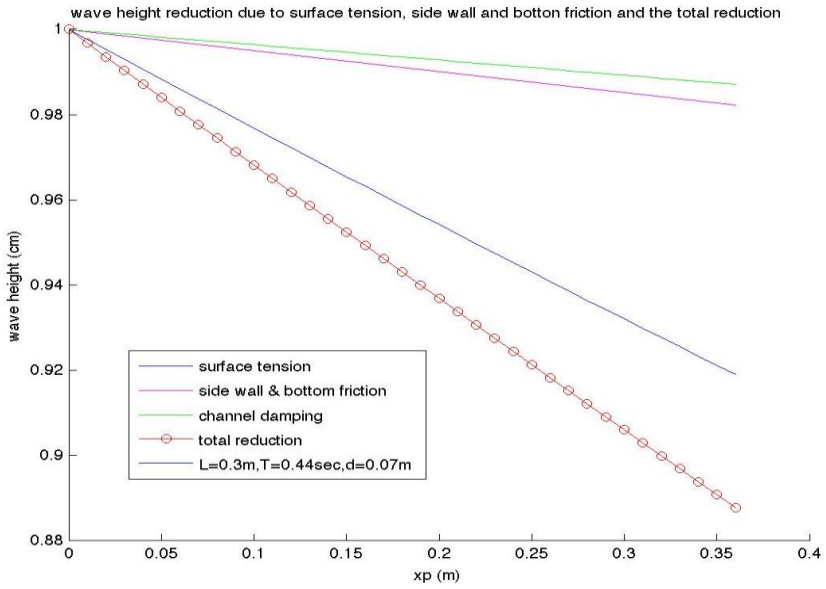

Figure 3.10: The wave height reduction in the deep-water part of the basin.

Figure 3.10 illustrates the wave height attenuation due to surface tension, the side wall and bottom friction and the wave attenuation in a channel due to internal friction (Kaulegan's equation). It is obvious that the most important wave attenuation is caused by the surface tension and for that reason it is examined below (figure 3.11).

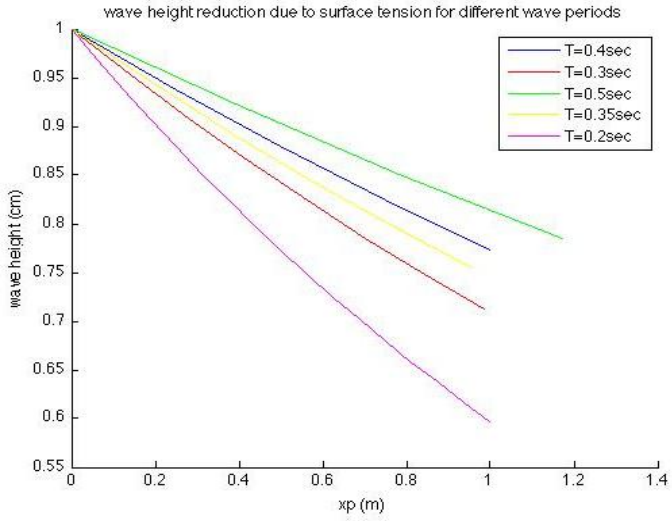

Figure 3.11: The wave height reduction due to surface tension effects for different wave periods (T).

According to the equation 11 of surface tension (page 39) the wave frequency and so the wave period is the key for the wave height reduction. Examining five different wave periods (figure 3.11) is obvious that the wave attenuation is greater as the wave period is decreasing. For example, for T=0.35sec the reduction due the surface tension effects is about 10%, while for T=0.2sec is 17%, when the waves travel in the deep part of the basin (x_p=0.35m).

Assuming that the breakwater is absent, applying the four wave height attenuation equations (11,15,16) along with the shoaling one (equation 8) for the whole basin (x_p=1.12m), the following wave height attenuation is plotted (figure 3.12). The wave is attenuated at the deep part of the basin and at the plateau, while the wave height is increasing due to shoaling at the area with the slope.

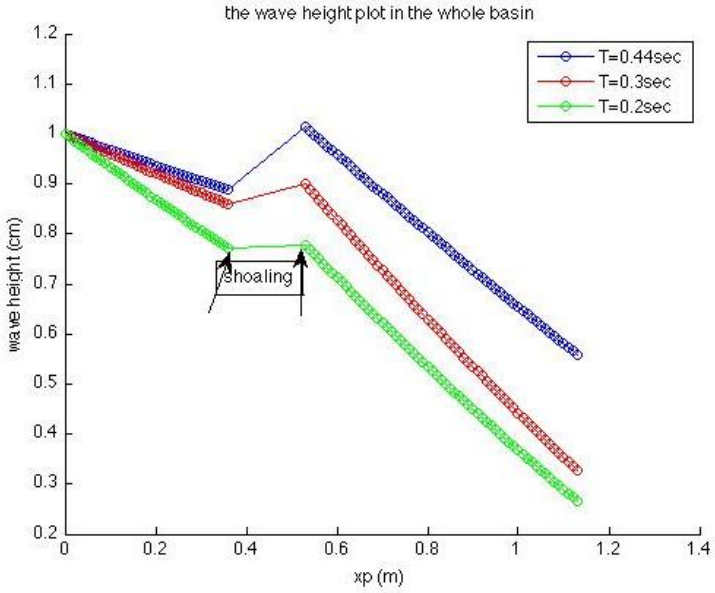

Figure 3.12: The wave height plot in the basin.

3.2 Breakwater gap

3.2.1 Micro models

The following figures 3.13 & 3.14 illustrate the 3D wave field in the experimental basin having a pair of breakwaters that create a gap in the middle.

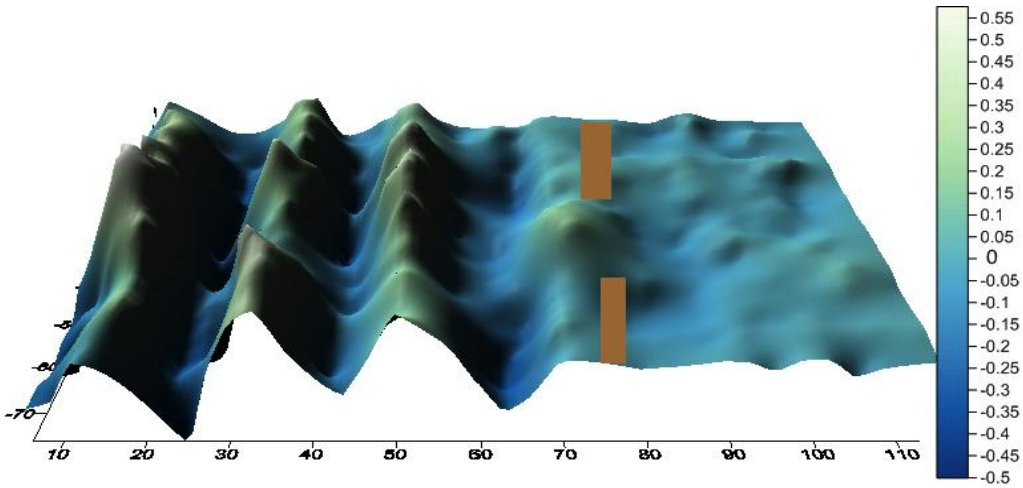

Figure 3.13: The wave propagating in the basin, interrupted by breakwaters. Wave characteristics: T=0.32sec, L= 0.15m and Hi=0.6cm (file name: run4gap70)

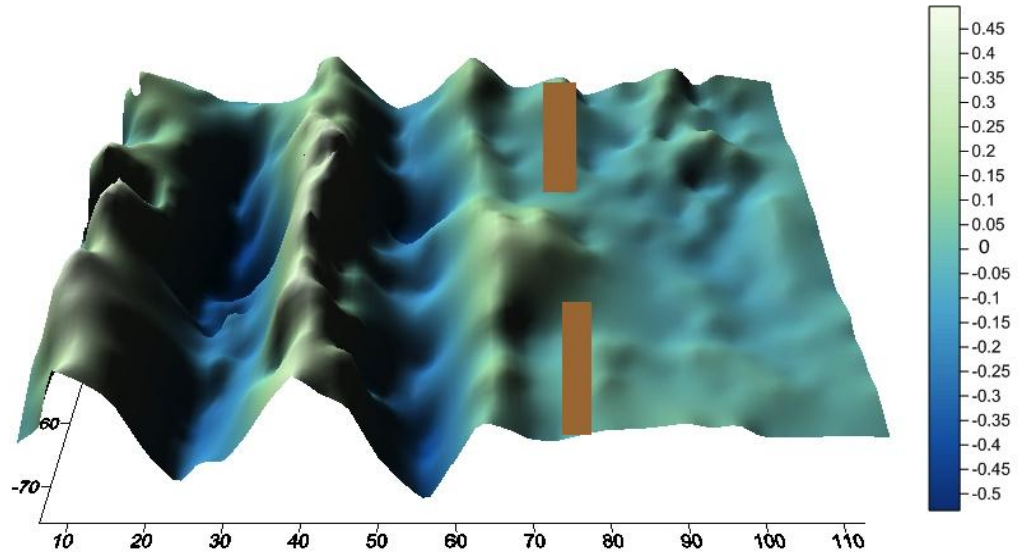

Figure 3.14: The wave propagating in the basin, interrupted by breakwaters. Wave characteristics: T=0.38sec, L= 0.22m and Hi=0.6cm (file name: run5gap70)

It can be seen that the wave field is much more easily destroyed than at the single breakwater. The wave height is reduced a lot in the sheltered area resulting in a small diffraction coefficient as it is reported in the next pages. The quick destruction of the wave field along with the small wave height makes it difficult to discern the crests and

troughs. Reflections that occur near the boundaries at the end of the basin increase the wave height corresponding to the increased diffraction coefficient.

Based on the experimental measurements (micro model), the analysis results in the following contours of equal diffraction coefficient at a breakwater gap (figure 3.15) and is compared to the theoretical diagram of Johnson (1952) (figure 2.12).

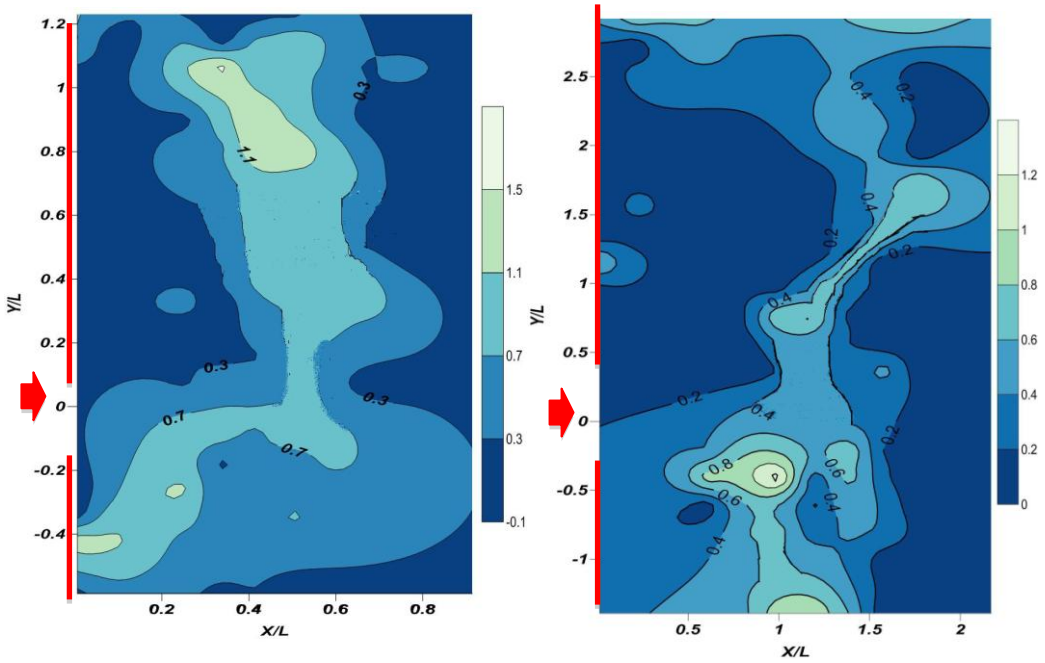

Figure 3.15: The experimental (micro model) contours of equal diffraction coefficient at a breakwater gap of B/L=0.57 (exp1) (left) and of B/L=1.34 (exp3) (right).

The breakwaters are located to the left (marked in red), the gap formed by those is B=21.5cm and the red vector shows the wave direction. In the sheltered area of the breakwater, the values of the diffraction coefficient (K') are in the expected range of 0.2-1[+]. The diffracted wave height just after the breakwater is greater than that at the end of the basin (in the case where two 'diffracted' crests occur in the sheltered area of the basin). Due to this, the diffraction coefficient ($K'=H_d/H_i$) is greater near the breakwater than further. A careful observation at the right figure indicates bigger values of the diffraction coefficient near the side walls. This happens as these boundaries cause the reflection of the wave that increases the wave height (H_d).

The main difference between the theoretical and experimental diagrams is as stated earlier, the size of the area under investigation. The theoretical graph of Johnson (1952), assumes an area of 20x20L, without any solid boundaries. In contrast, the size of the micro modeled experimental area is 2x3L and is surrounded by the basin walls and at the end energy absorbing gravel beach exists. This implies that all the residual wave-boundary interactions, like wave reaction, are not considered.

The measured values of the diffraction coefficient reduce much faster along the area's

length than the theoretical ones. For example (figure 3.15 right), within the distance of 2L the experimental coefficient has reduced to approximately 0.2, while its theoretical value is around 0.5. The rate of energy reduction inside the protected area is larger in the micro-model.

To conclude, when comparing the micro model to the numerical model and the theory it is subjected to errors introduced due to the presence of solid boundaries in the micro model, which result in unwanted interactions with the diffracted waves such as wave reaction.

3.2.2 Mike 21

This vastly used numerical model was also used to model the experiment where the waves travel through a breakwater gap. Figure 3.16 shows the isolines of the wave disturbance coefficient in the basin.

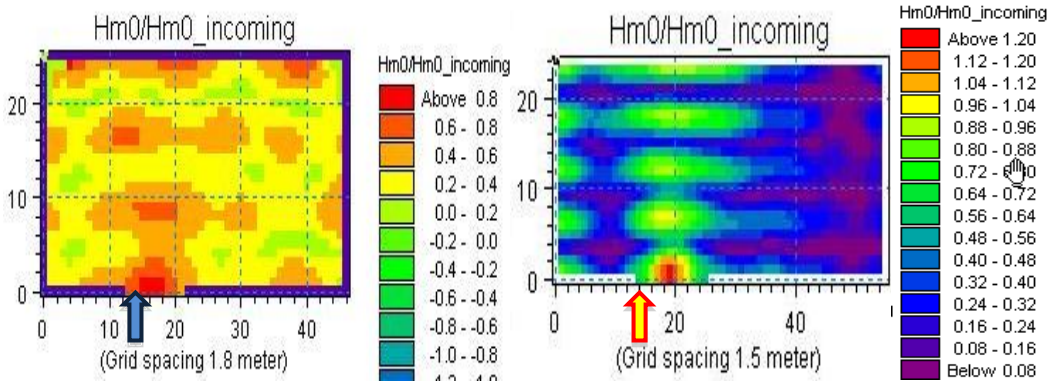

Figure 3.16: The diffraction coefficient (K'=Hd/Hi) extracted by the software for a breakwater gap. Left: exp1; L= 0.38m and right: exp5; L=0.2m (water depth d=0.075m).

The modeled area was rotated 90^{o} anti clockwise and the vectors show the wave direction. The numerical values of the diffraction coefficient agree with the experimental ones and are lower than unity even in the unsheltered area. The numerical and experimental values are smaller than the theoretical ones for the reasons that were explained earlier.

3.3 Conclusion

Overall, considering all the results it can be concluded that wave diffraction through a single breakwater and a breakwater gap can be modeled to an acceptable level using micro-models. Micro-models along with the PIV mapping method can provide the temporal and spatial history of the evolution of a wave field within the full dimensions of a physical model. Laboratory effects that are the cause of the small dimensions of the wave basin, bias the final result. Similar investigations can be better facilitated in a larger and wider basin. During the current experimental series the following laboratory effect was observed; although waves transfer energy they can also, depending on their steepness, transfer mass (water and PIV particles) to the end of the basin.

An unwanted surface flow drift was observed and was attributed to the combination of:

1. The movement of mass by steep waves.
2. The presence of a structure inside the basin.
3. The small size of the basin. Such a flow pattern affects the quality of the final result, limits the experimental time and could be developed in any 3D wave facility.

Although the development of such a drift is enhanced by the small size of the current basin it is possible that a similar flow pattern will develop in any large scale 3D facility and locally increase the water level.

4. Ostia-Rome yacht harbor

As it was stated before, it is important to consider the diffraction characteristics, in order to successfully design a port. The proposed layout of the harbor must be able to reduce the incoming wave height. Numerical models, as reported by scientists cannot describe with accuracy the highly non-linear processes between the waves and the design of the port, or need a large and expensive computational effort. For that reason, physical models are only able to describe those non-linear processes, but the construction and experimental cost is high. The answer to that may be the use of micro models.

4.1 The experimental solution using Micro models

For the reasons stated above, Stagonas (2010) selected the Ostia-Rome yacht harbor for the study of wave diffraction using micro models, due to its impressive, innovative and complex shape. The purpose of the physical micro-model is to simulate the wave diffraction phenomenon and investigate whether wave micro-models can be the tool for testing different design scenarios. The unique design of the port has two rubble mound breakwaters that converge to the entrance, to form an elliptic-shaped outer harbor (figure 4.1). A gravel beach (incline 1:3) located opposite to the entrance is used to absorb some of the wave energy.

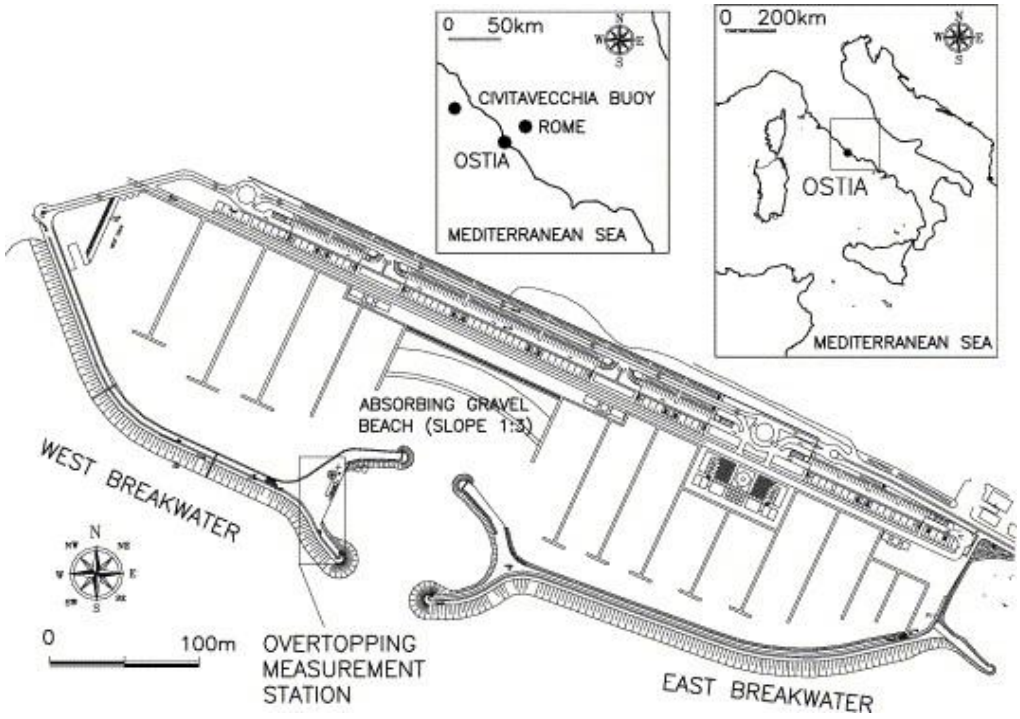

Figure 4.1: The location and layout of the harbour (Bellotti, G. (2007).

Stagonas (2010) modeled the port as it is shown in the figure 4.2-4.4 below. As in the previous models and so in this one, the PIV method was used to map the wave field evolution within the basin. This time, each frame has a resolution of 1920x1080p that allows the mapping of a larger area with a denser interrogation grid. Surface elevation was measured by five resistance type wave probes at 10 different locations in and out of the area of the harbor, in order to compare it to the wave field evolution and surface elevation, mapped and measured, with the PIV method as described earlier. Having a 4m-water depth in the real situation, corresponds to 0.025m in the model, as according to the literature is required in order to avoid the scale effects. That results in a scale of 1:163. Froude's law was used to calculate all the other model dimensions required. The seabed of the model contains a 1:6 slope and a plateau (figure 4.2). The waves approach the breakwater at an angle of 90^{o}. Two different design scenarios are tested using the micro-models, in order to study their effectiveness. The first scenario contains only the two front breakwaters (figure 4.3) and the second has two more rear, curved elements to form a secondary harbour in order to reduce the transmitted wave energy (figure 4.4).

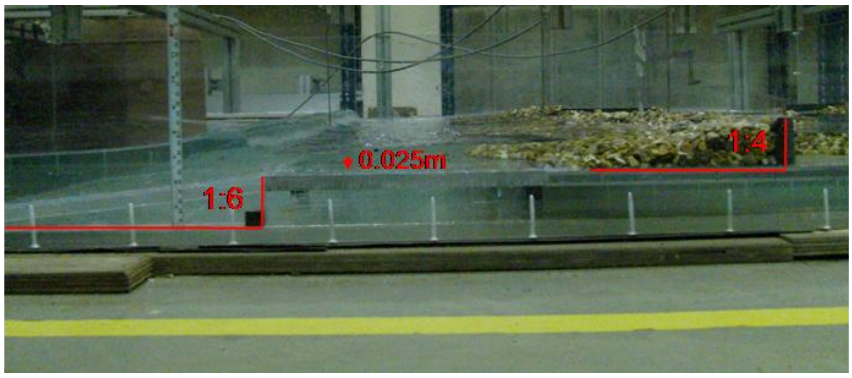

Figure 4.2: The harbor's bed and bathymetry.

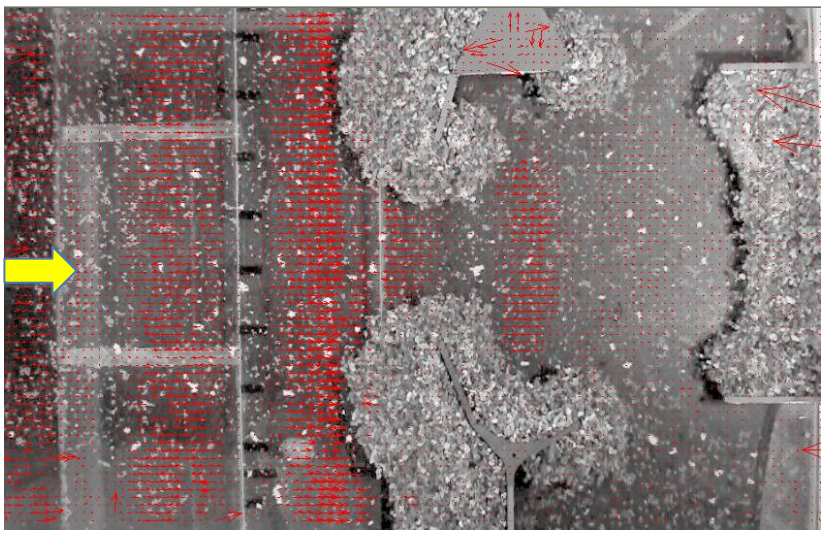

Figure 4.3: The layout of the Ostia port when half of the breakwaters are in place (scenario1)

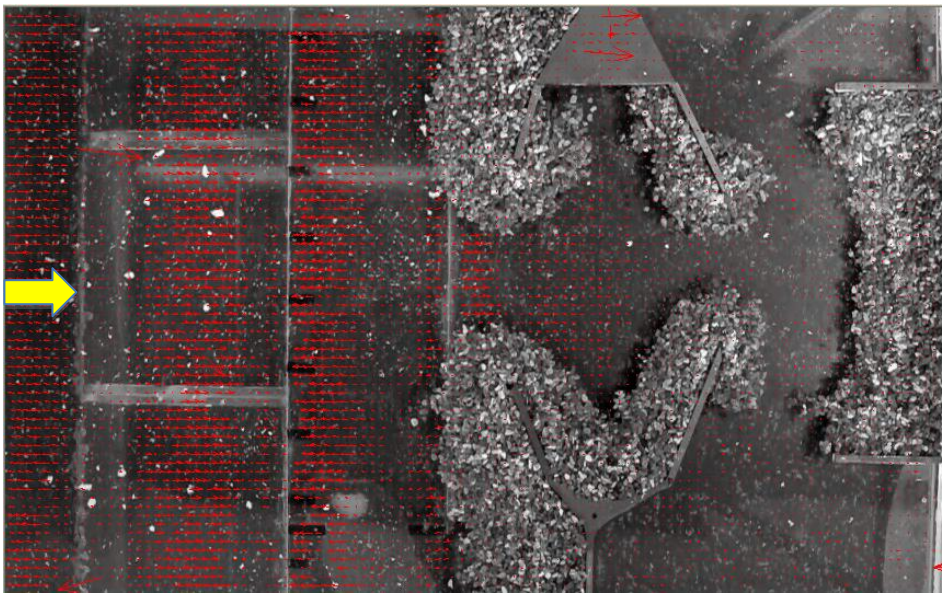

Figure 4.4: The layout of the Ostia port when all the breakwaters are in place (scenario2).

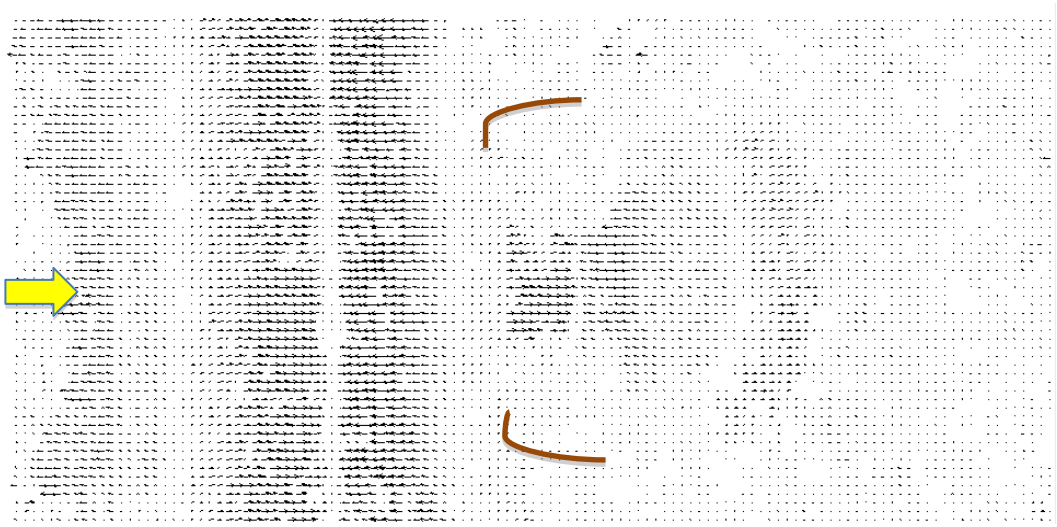

Figure 4.5: The Ostia port vector map for scenario 1.

The incident wave height is calculated just before the entrance of the harbor, as the average wave height of all the particles that are in the same position in the x-axis (have the same value on the x-axis).

Table 4.1: The experimental conditions of the Ostia port.

Ostia port	d (mm)	Hi (cm)	L (m)	T (sec)
Exp 7 scenario 1	25	1.3	0.72	0.67
Exp 6 scenario 1	25	0.4	0.55	0.58
Exp 3 scenario 2	25	0.8	0.75	0.68
Exp 4 scenario 2	25	0.7	0.60	0.62

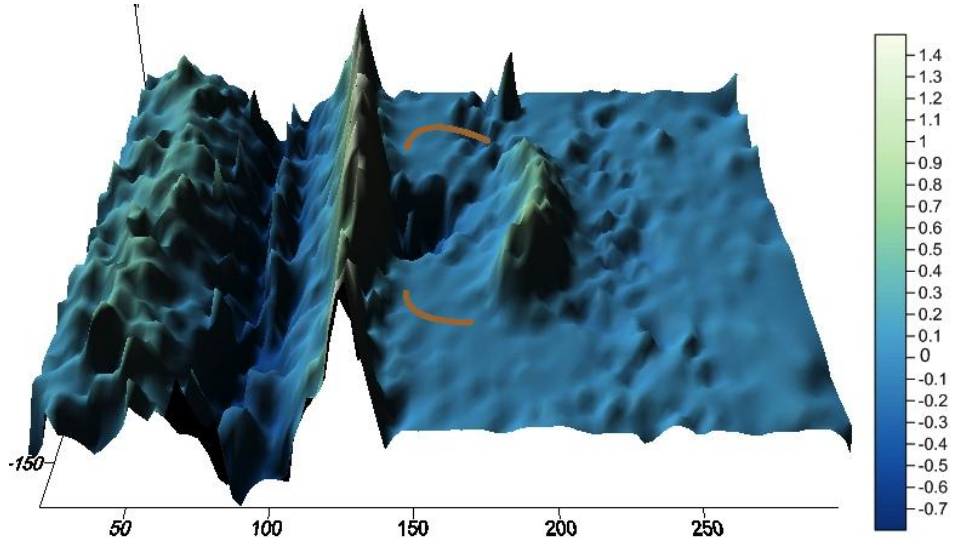

Figure 4.6: The Ostia port modeled (scenario 1); waves propagating having the following characteristics: L=0.72m, Hi=1.3cm, T=0.67 sec (exp 7).

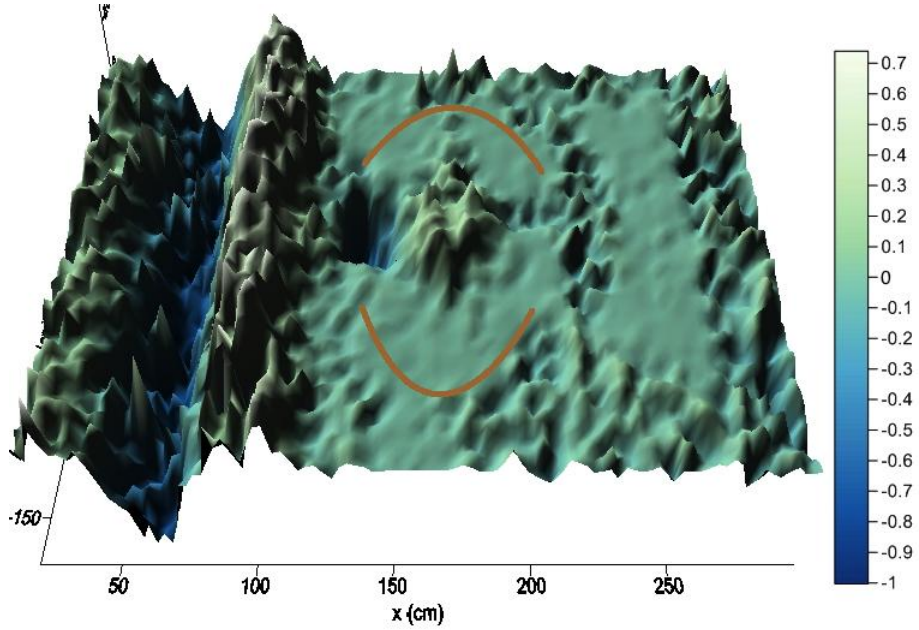

Figure 4.7: The Ostia port modeled (scenario 2); waves propagating having the following characteristics: L=0.75m, Hi=0.8cm, T=0.62 sec (exp 3).

The velocity vector field is illustrated in the previous figures (4.3 – 4.5) in both scenarios and the extracted 3D Surface elevation field in figures 4.6 & 4.7. The wave height reduction is obvious in both occasions, but when all the breakwaters are in place the reduction is bigger. Reflection occurs near the boundaries that increase the diffracted wave height, as figure 4.7 illustrates.

4.2 The probe measurements

The wave height is also measured in every location using the probes located in the wave basin (figure 4.8) in order to compare the measurements with the experimental (micro modeled) ones. Stagonas provided the data of his experiments.

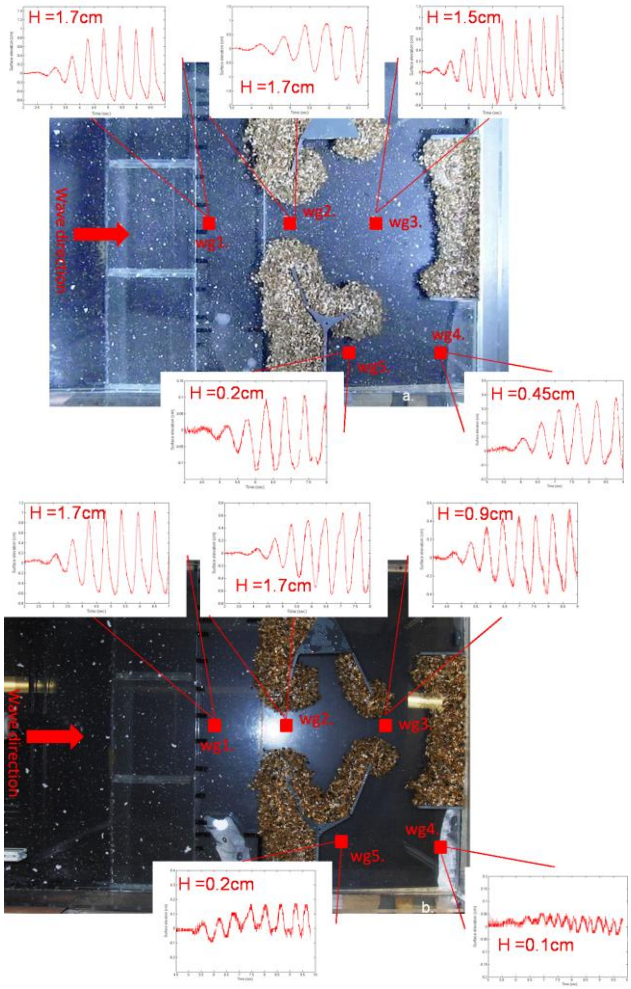

Figure 4.8: Wave probe locations and recorded surface elevation (wave height) for: a. design scenario 1, and b. design scenario 2. (Stagonas 2010)

Table 4.2: The diffraction coefficient at the different locations in the basin for the probe measurements.

	Hi probe (cm)	Hd wg3 (cm)	K' wg3	Hd wg4 (cm)	K' wg4	Hd wg5 (cm)	K' wg5
Scenario 1	1.7	1.5	0.88	0.45	0.26	0.20	0.12
Scenario 2	1.7	0.9	0.53	0.10	0.06	0.20	0.12

The probe measurements show a wave height reduction at about 1-(1.5/1.7)= 12% at the entrance of the harbor and 1-(0.45/1.7)=84% at the inside the harbor, for the first scenario. When the secondary breakwaters are put in place (scenario2) the reduction of the wave height is bigger, 1-(0.9/1.7)=47% in the entrance and 1-(0.1/1.7)=94% inside the harbor (figure 4.8).

Table 4.3: The experimental diffraction coefficient at the different locations in the basin results

	Hi m-m (cm)	**Hd wg3 (cm)**	**K' wg3**	**Hd wg4 (cm)**	**K' wg4**	**Hd wg5 (cm)**	**K' wg5**
Scenario 1	1.62	1.1	0.68	0.22	0.14	0.45	0.28
Scenario 2	1.77	0.77	0.44	0.10	0.06	0.22	0.12

Micro modeling using PIV estimates the reduction (diffraction coefficient $K'=H_i/H_d$) as in table 4.3. In the same way, the wave height reduction is about 32% at the entrance of the harbor and 86% at the inside the harbor, for the first scenario. For the second scenario the reduction of the wave height is bigger; 56% in the entrance and 1-(0.1/1.7)=94% inside the harbor.

According to the results, the experiment (micro models) along with the probe measurements show that the wave energy transmitted inside the harbor is significantly reduced by the presence of the breakwaters (scenario 1). The reduction is even bigger when the two secondary breakwaters are put in place (scenario 2). The Surface flow velocities are reduced along with the disturbance of the water surface, which only occurs at the exit of the secondary harbor. Since the wave energy is a function of the wave height squared ($E=\rho_w g H^2/8$), the energy transmitted into the primary harbour is decreased 54% for the first scenario and 82% for the second (experimental) while the probe measurements give 22% and 72% respectively.

4.3 The numerical solution - Mike21

Mike 21 is used to simulate the diffraction process in this unique port. The model layout is illustrated in the following figure (4.9). What happens in the area behind the breakwaters has no influence on the main area of interest and so these two areas are turned into artificial land without affecting the accuracy of the results and also saves computation time. Those areas are marked in red color in the following figure,

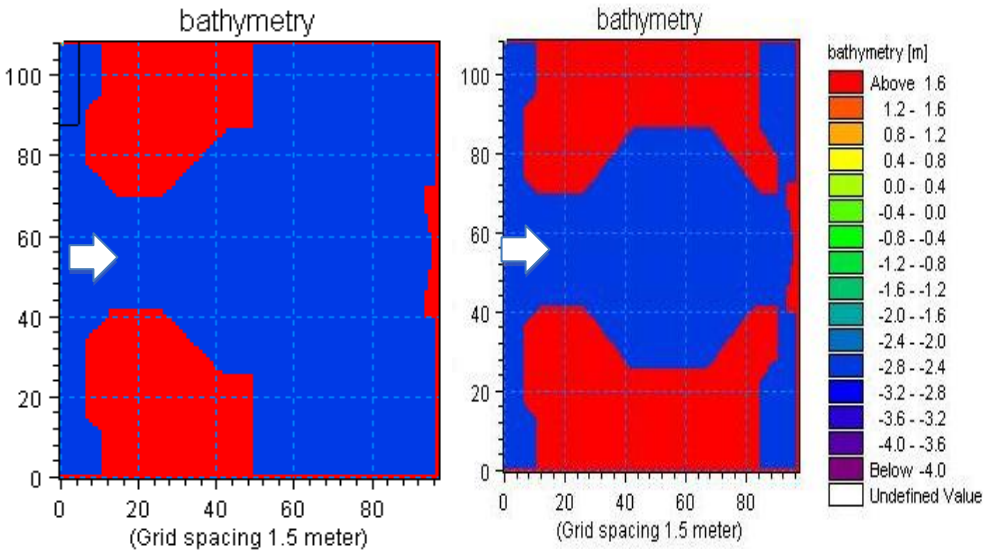

Figure 4.9: The model layout of the Ostia port, scenario 1(left) and scenario 2 (right).

The isolines of the wave disturbance coefficient in Ostia port are plotted below for both scenarios.

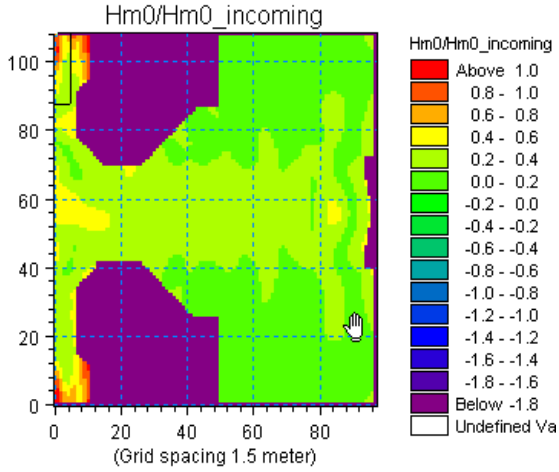

Figure 4.10: The diffraction coefficient (K'=Hd/Hi) of the Ostia port for the first scenario (exp7; L= 0.72m, Hi=1.3 cm, water depth d=0.025m).

When half of the breakwaters are in place (figure 4.10), the diffraction coefficient on the side of the basin is about 0.2, while in the middle of it is between 0.2 and 0.4. The unique layout of the port causes the strong reduction of the have height, so the area is sheltered from extreme events.

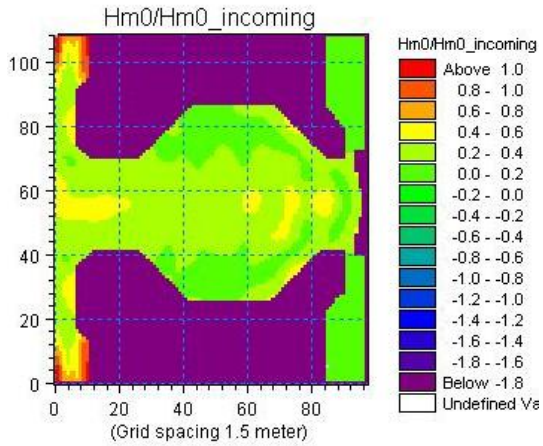

Figure 4.11: The diffraction coefficient (K'=Hd/Hi) of the Ostia port for the second scenario (exp3; L= 0.75m, Hi=0.8 cm, water depth d=0.025m).

When all of the breakwaters are in place (figure 4.11), the diffraction coefficient on the side of the basin is again around 0.2, while in the middle of it is between 0.2 and 0.4. The bigger value of the diffraction coefficient in front of the second pair of the breakwaters is due to the increased wave height, as caused by the reflection from the breakwater.

Table 4.4: The experimental numerical and measured diffraction coefficient (K')

Scenario	K' wg3 probe	K' wg3 exp	K' wg3 num	K' wg4 probe	K' wg4 exp	K' wg4 num	K' wg5 probe	K' wg5 exp	K' wg5 num
1	0.88	0.68	0.53	0.26	0.23	0.18	0.12	0.28	0.17
2	0.53	0.44	0.51	0.06	0.18	0.15	0.12	0.12	0.13

To sum up, the qualitative agreement between the three methods is satisfactory. It is highly possible that the use of the linear wave theory for the conversion of flow velocities to surface elevation is responsible for the observed quantitative differences. The present shape of the Ostia-Rome yacht harbor was found to be more efficient on reducing the energy transmitted inside the inner basin.

The results encourage the use of wave micro-models for the design of coastal structures. Using micro-models along with the PIV gives a good estimation of the magnitude of the surface flow inside the basin, although is not 100% accurate. PIV provides a full field surface flow and elevation data while micro-models minimize the experimental time, cost, and effort and staff requirements. In summary the use of micro-models along with the PIV mapping method indicates that the design of the Ostia yacht harbor is the most effective as it reduces the transmitted wave energy.

5. Conclusion

The present project is investigating the validity and potentials of very small-scale physical models of water waves, called micro-models for the diffraction phenomenon. If micro models are valid, then they can be a cheap and quick tool to study and pre-design large scale physical models.

Reviewing the literature, it can be concluded that non-breaking waves can be modeled at very small scales when the water depth is d > 0.02m and the wave period is T > 0.35sec where the scale effects are small and can be neglected. Then the micro modeling of water wave propagation and diffraction is valid.

Stagonas (2010) was the first to study micro modeling of wave fields for coastal engineering purposes, using a novel wave field mapping method that allows the full three-dimensional mapping inside a small-scale wave basin. This technique, called Particle Image Velocimetry, provides a very good overview of the temporal and spatial wave field evolution. Using the linear wave theory, the mapping method gives a satisfactory estimation of the magnitude of non-linear wave-structure interactions such as wave diffraction. In order to study the validity of the diffraction phenomenon when using micro models, the experimental results of micro models are compared to those given by the theoretical (Penny & Price 1952) and numerical (Mike 21 BW) solution. The thesis examines the wave diffraction around a single breakwater and a breakwater gap. The unique designed Ostia-Rome port was also modeled using micro models and the numerical model Mike 21 BW. The diffraction coefficient is calculated using the three methods for the three different layouts previously mentioned.

The conclusions are the following:

- For the case of the single breakwater, a good agreement is observed between the three methods. The experimental and numerical deviations from the theoretical values of the diffraction coefficient occur mostly near the boundaries (at the position of $\theta o = 135 \circ$) of the basin and are the cause of reflection on the side walls. In addition, the linear wave theory used to convert the flow velocities to surface elevation is responsible for the observed quantitative differences.
- The diffraction coefficient, when waves pass through a breakwater gap, reduces much faster along the experimental basin than the theoretical. The rate of reduction in micro model and numerical model is larger than the theoretical. Further study is required for both the single breakwater and the gap, as the literature cannot estimate the coefficient in that small scale.

- The mapping method was improved, comparing to the previous studies, as the reflection from the breakwater is taken into account when calculating the wave height.
- The wave damping that occurs in the experimental basin reduces the wave height up to 11% in the deep part of the basin. Surface tension is the most important factor that reduces the wave height. The key in the equation of surface tension is the frequency and thus the wave period, and so: the smaller the wave period the bigger the reduction.
- A bigger micro model was used to study the diffraction phenomenon for the Ostia port that has a unique design. Strong reduction of the have height (32% for the first scenario and 56% for the second) occurs and the transmitted wave energy is reduced up to 82% in micro models. The experimental wave height of Ostia port is compared to the probes' measurements. A good agreement is observed when comparing the diffraction coefficient of the three methods.
- Comparing to the large scale physical models, micro models have really little money and time requirements and there is no need for large space, technical and experimental staff. Wave micro-models can be an interesting way of investigating coastal engineering problems such as the wave propagation and diffraction and prepare large-scale experiments. Using wave micro-models along with theoretical and numerical models can be with no doubt a useful and reliable tool for the diffraction analysis.

6. References

Abul-Azm A. J. and Williams A. N (1995). Oblique wave diffraction by segment offshore breakwaters.

Beckett, A. and Marshall, S. (1983). Design and construction of muara deep water port, Brunei., Proc. of the Inst. of Civil Eng. London. Available at:

Beckett, T. (1992). Hydraulic mini-models studies, Proc. of the 2nd Intern. Conf. in Marina Technology, pp. 283

Biesel, F. (1949) Calcul de l'ammortissementd'unehouledansunliquidevisqueux de profondeurfinie. La Houille Blanche. 4

Blue, F. and Johnson, J. (1949). Dffraction of water waves passing through a breakwater gap, Trans. Amer. Geophys. Union 30: 705-718.

Briganti, R., Belloti, G., Frano, L., De Rouck, J. and Geeraerts, J., Marc Willems (2008). Prototype measurements and small-scale model tests of wave overtopping at shallow rubble-mound breakwaters: the Ostia-Rome yacht harbour case.

Briggs MJ, Thompson EF, Vincent CL (1995). Wave diffraction around breakwater. J. Waterway, Port, Coastal, Ocean Eng., ASCE 121(1): 23-35.

Carr, J.H., and Stelzriede, M.E. (1951). Diffraction of water waves by breakwaters: Presented at symposium on gravity waves, National Bureau of Standards, Washington, D.C., June 18-20, 1951.

Claude Strauser, Chief of Potamology Section, St. Luis army engineer district: ESPRIT (February 1998). Available online at:
http://www.mvs.usace.army.mil/pa/esprit/1998/esp9802.pdf

Costa F.V 1981. Forces Associated to different fluid properties as affected by scaling. Costal Engineering Vol. 5, pp 371-377.

Costa F.V 1984. The modeling of non uniform and of unsteady flow. Symposium on scale effects in modeling hydraulic structures, e.d.H.Kobus, international association of hydraulic research pp 3.1-1- 3.1-6.

Costa F.V 1990.Time scale selection in hydraulic modeling.Journal of coastal research Vol. 7 pp 29-40.

Dalrymple, R. (1985). Physical modeling in Coastal Engineering.

Dalrymple, R.A. and Martin, P.A. 1990. Wave Diffraction Through Offshore Breakwaters. Journal of Waterway, Port, Coastal and Ocean Engineering, ASCE 116, 727-741.

Davinroy Robert D., David C. Gordon, Robert D. Hetrick, Sedimentation study of the Mississippi river Sante Fe Chute, Doolan Chute hydraulic micro model investigation. U.S. Army Corps of Engineers, St. Louis District, Technical Report M1, September 1996.

Dong Jun; Qi Jianxia; Miao Runcai (2007); Measurement of the damping of liquid surface wave by diffraction method. Brazilian Journal of Physics, vol. 37, no. 3B.

Dunham D. James; Refraction and diffraction diagrams. USACE, L.A California USA.Available online at: http://journals.tdl.org/ICCE/article/viewFile/907/004_Dunham

Chief, Beach Erosion Unit, Los Angeles District California, Corps of Engineers

Ettema, R. (2001). A framework for evaluating micro-models, Technical report, Limited Distribution Report No. 295, Iowa Institute of Hydraulic Research, The University of Iowa, Iowa City, Iowa.

Ettema, R., Fujita, I., Muste, M. and Kruger, A. (1997). Particle image velocimetry for whole field measurement of ice velocities, Cold Regions Science and Technology 26: 97-112.

Ettema, R. and Maynord, R. (2002). Framework for evaluating very small hydraulic models of channel - control works, Technical report, Hydraulic Measurements and Experimental Methods, ASCE, Reston, U.S.

Ettema, R. and Muste, M. (2004). Scale effects in flume experiments on flow around a spur dike in at bed channel, Journal of Hydraulic Engineering 130(7): 635-646.

Falvey, H. T (1999). Letter to editor, 'Missuse of term model.' Civil engineering magazine, ASCE, Reston, Va., Vol. 69, No. 12, December.

Fujita, I., Muste, M. and Kruger, A. (1998). Large scale particle image velocimetry for flow analysis in hydraulic engineering applications, Journal of Hydraulic Research 36: 397-414.

Goda, Y., Yoshimura, T. and Ito, M. (1971). Reflection And Diffraction Of Water Waves By An Insular Breakwater, Report of The Port and Harbor Research Institute of Japan, 10, 4-51.

Gray, C. and Bruce, T. (1995). The application of particle image velocimetry (PIV) to offshore engineering, Proceedings of the 5th Int. Offshore and Polar Eng. Conf., ISOPE'95, Vol. 3, pp. 701-708.

Hughes, S. (1993). Physical models and laboratory techniques in coastal engineering, World Scientific.

Hunt, J. (1952). Viscous damping of waves over an inclined bed in a channel of infinite width, La Houille Blanche **7**: 836.

Huygens, M. and Verhoeven, R. 1992. Wave Diffraction Patterns Around Isolated Offshore Structures, Proc. Second Int. Conf. on Marina Technology, Southampton, U.K., 197-212.

Johnson, J. (1952). Generalized wave diffraction diagrams, Proc. Second Conf. Coastal Eng. Berkeley, Calif.: The Eng. Foundation Council on Wave Research, pp. 6-23.

Keulegan, G. (1950a). The gradual damping of a progressive oscillatory wave with distance in a prismatic rectangular channel, Technical report, (unpublished-in Hughes 1993) National Bureau of Standards, Washington D.C.

Keulegan, G. (1950b). Wave motion, J. Wiley & Sons, pp. 711-768.

Kim S.D and Lee H.J (2010). The comparison of analytical and numerical solutions for wave diffraction due to insular breakwater.

Kim S.D and Lee H.J (2009). Diffraction Analysis by Gap Type Breakwater Using Polynomial Approximation for Fresnel Integrals.

Lamb, H. (1932). Hydrodynamics. Cambridge University Press, Cambridge, England.

Larras, J. (1966). "Diffraction de la houle par les obstacles rectilignes semi-indefinis sous incidence oblique," Cah. Oceanograph., 18, 661-667.

LeMehaute, B. (1990). 'Similitude' in ocean engineering Science, Vol 9; Part B in the series The Sea, John Wiley and sons, New York pp 955-980.

LeMehaute, B. (1965). On the Froude-Cauchy Similitude, Santa Barbara coastal engineering specialty conference, Chap. 14, p.p 327-343.

LeMehaute, B. (1976). Similitude in coastal engineering, Journal of waterways, harbors and coastal engineering division 102.

Madsen, P A, Sørensen, O R and Schäffer, H A (1997a); "Surf zone dynamics simulated by a Boussinesq type model. Part I: Model description and cross-shore motion of regular waves". Coastal Eng., 32, 255-288. (1997b), Part II: Surf beat and swash zone oscillations for wave groups and irregular waves". Coastal Eng., 32, 289-320.(1992), "A new form of the Boussinesq equations with improved linear dispersion characteristics. Part 2: A slowly varying Bathymetry". Coastal Eng., 18, 183-204. (1991); (Part 1); Coastal Eng., 15, 371-388.

Maynord, S. (2006). Evaluation of the micromodel: an extremely small-scale moveable bed model, Journal of Hydraulic Engineering. 132: 343-353.

Maziar Hemati; Micro-Particle Image Velocimetry, MAE 199, (2007).

Memos, CD, "Diffraction of Waves Through a Gap Between Two Inclined Breakwaters," Ph.D. Thesis, University of London, London, England, 1976.
Memos, CD., "An Extended Approach to Wave Scattering Through a Harbor Entrance," Bulletin of the Permanent International Association of Navigation Congresses, Vol. I, No. 35, 1980a, pp. 20-26.
Memos, CD., "Energy Transmission by Surface Waves Through an Opening," Journalof Fluid Mechanics, Vol. 97, Pt. 3, 1980b, pp. 557-568.
Memos, CD., "Water Waves Diffracted by Two Breakwaters," Journal of HydraulicResearch, Vol. 18, No. 4, 1980c, pp. 343-357.

Nece, R. (1985). Physical Modelling of Tidal Exchange in Small-Boat Harbors, Numerical and Physical Modelling of Ports and Harbors, Birmingham, England, Dept. of Civil Engineering of Brimingham University and International Association for Hydraulic Researsh.

Oumeraci, H. (1984). Scale effects in coastal hydraulic models, Proc. Symposium on Scale Effects in Modeling Hydraulic Structures, IAHR.

Penny, W. and Price, A. (1944). Diffraction of sea waves by breakwaters, Technical report, Directorate of miscellaneous weapons development, Technical History No. 26, Artificial Harbors, Sec. 3D.

Penny, W. and Price, A. (1952). The diffraction theory of sea waves by breakwaters, and the shelter afforded by breakwaters, Phi. Trans. Royal Soc. (London) 244: 236- 253.

Pos J.D and Kliner F.A (1984). Breakwater gap wave diffraction: an experimental and numerical study.

Putnam, J. and Arthur, R. (1948). Diffraction of water waves by breakwaters, Trans. Amer. Geophys. Union pp. 481-490.

Schüttrumpf Holger and Oumeraci Hocine; Scale and Model Effects in Crest Level Design; available at: http://www.itv.is/ics2005/Data/B2.1/schuettrumpf_PA.pdf. Pictures from: Schüttrumpf, H., 2001. WellenüberlaufstrmungbeiSeedeichen – Experimentelle und
TheoretischeUntersuchungen. PHD-Thesis.

Schwinger, J., and Saxon, D. S. (1968). Discontinuities in waveguides: notes on lectures by Julian Schwinger. Gordon and Breach Sci. Pub., New York, N.Y.

Shore Protection manual (SPM) (1984); Vol I; Coastal Engineering Research Center; US Army Corps of Engineers; Washington; Waterways Experiment Station.

Silvester, R., and Lim, T. (1968). "Application of wave diffraction data," Proc. 11th Inter. Conf. Coast.Engrg., London, England, 248-270.

Sørensen, O R, Schäffer, H A and Sørensen. L S (2004), "Boussinesq type modeling using an unstructured finite element technique". Coastal Eng., 50, 181-198.

Sommerfeld A (1986). Mathematischetheoriedier diffraction. Math. Annalen. 47: 317-374.

Stagonas D. and Muller G. (2006). Wave field mapping with particle image velocimetry.

Stagonas, D., 2006.Micro modeling of wave fields. M.Sc. Thesis, University of Southampton.

Stagonas D. 2010. Micro modeling of wave fields. PhD. Thesis, University of Southampton.

Suh K-D., Kim H., 2008. Water wave scattering by partially reflecting breakwaters. KSCE Journal of Civil Engineering 12(2), 71–76.

Suh K-D., Kim H., Do K.D 2010. Scattering of obliquely incident water waves by partially reflecting non-transmitting breakwaters.

Svendsen, I. (1985). Physical modeling of water waves. In Physical modeling in coastal engineering, Rotterdam: A.A Balkema, Inc., chapter 2, pp. 13-45.

Svendsen, I. and Haas, K. (1999). Interaction of undertow and rip currents, In Proc. Vth COPEDEC, Cape Town, Vol. 1, pp. 218-229.
Tirindelli, M., Lamberti, A., Paphitis, D., Vidal, C., Hawkins, S., Morchella, P. and Sanchez-Arcilla, A. (2000). Wave action on rubble mound breakwaters: the problem of scale effect, Technical report, DELOS EVK3-CT-2000-00041.

Wiegel, R. (1962); Diffraction of waves by semi-infinite breakwater, J. Hyd. Div., Proc. ASCE 88: 27-44.

Wiegel, R. (1976); Oceanographical engineering.

Y. -X. Yu, S. -X. Liu, Y.S. Li, Onyx W.H. Wai. Refraction and diffraction of random waves through breakwater.

Yalin, M. S. (1971). 'Theory of hydraulic models'. McMillan, London.

Yalin, M. S. (1989). 'Fundamentals of Hydraulic Physical Models', recent Advances in Hydraulic Physical Models, R. Martins, Ed, Kluwer Academic Publishers, Dordrecht, The Netherlands pp 567-588.

Word count: 18540